International Journal of Nanomedicine

Dovepress
open access to scientific and medical research

Open Access Full Text Article

ORIGINAL RESEARCH

A Novel Therapeutic siRNA Nanoparticle Designed for Dual-Targeting CD44 and Gli1 of Gastric Cancer Stem Cells

This article was published in the following Dove Press journal:
International Journal of Nanomedicine

Hongjuan Yao[1]
Lan Sun[2]
Jingcao Li[2]
Xiaofei Zhou[1]
Rui Li[1]
Rongguang Shao[1]
Yingge Zhang[2]
Liang Li[1]

[1]Key Laboratory of Antibiotic Bioengineering of National Health and Family Planning Commission (NHFPC), Institute of Medicinal Biotechnology (IMB), Chinese Academy of Medical Sciences and Peking Union Medical College (CAMS & PUMC), Beijing 100050, People's Republic of China; [2]Key Laboratory of Nanopharmacology and Nanotoxicology, Beijing Institute of Pharmacology and Toxicology, Beijing 100850, People's Republic of China

Correspondence: Liang Li
Key Laboratory of Antibiotic Bioengineering of National Health and Family Planning Commission (NHFPC), Institute of Medicinal Biotechnology (IMB), Chinese Academy of Medical Sciences and Peking Union Medical College (CAMS & PUMC), Beijing 100050, People's Republic of China
Tel +86 10-63165824
Fax +86 10-63027302
Email liliang@imb.pumc.edu.cn

Yingge Zhang
Beijing Institute of Pharmacology and Toxicology, 27 Taiping Road, Haidian, Beijing 100850, People's Republic of China
Tel +86 10-66930654
Fax +86 10-68211656
Email zhangyg58@126.com

Purpose: Gastric cancer stem cells (CSCs) are important for the initiation, growth, recurrence, and metastasis of gastric cancer, due to their chemo-resistance and indefinite proliferation. Herein, to eliminate gastric CSCs, we developed novel CSC-targeting glioma-associated oncogene homolog 1 (*Gli1*) small interfering RNA (siRNA) nanoparticles that are specifically guided by a di-stearoyl-phosphatidyl-ethanolamine- hyaluronic-acid (DSPE-HA) single-point conjugate, as an intrinsic ligand of the CD44 receptor. We refer to these as targeting Gli1 siRNA nanoparticles.

Methods: We used the reductive amination reaction method for attaching amine groups of DSPE to aldehydic group of hyaluronic acid (HA) at the reducing end, to synthesize the DSPE-HA single-point conjugate. Next, targeting Gli1 siRNA nanoparticles were prepared using the layer-by-layer assembly method. We characterized the stem cellular features of targeting Gli1 siRNA nanoparticles, including their targeting efficiency, self-renewal capacity, the migration and invasion capacity of gastric CSCs, and the penetration ability of 3D tumor spheroids. Next, we evaluated the therapeutic efficacy of the targeting Gli1 siRNA nanoparticles by using in vivo relapsed tumor models of gastric CSCs.

Results: Compared with the multipoint conjugates, DSPE-HA single-point conjugates on the surface of nanoparticles showed significantly higher binding affinities with CD44. The targeting Gli1 siRNA nanoparticles significantly decreased Gli1 protein expression, inhibited CSC tumor spheroid and colony formation, and suppressed cell migration and invasion. Furthermore, in vivo imaging demonstrated that targeting Gli1 siRNA nanoparticles accumulated in tumor tissues, showing significant antitumor recurrence efficacy in vivo.

Conclusion: In summary, our targeting Gli1 siRNA nanoparticles significantly inhibited CSC malignancy features by specifically blocking Hedgehog (Hh) signaling both in vitro and in vivo, suggesting that this novel siRNA delivery system that specifically eliminates gastric CSCs provides a promising targeted therapeutic strategy for gastric cancer treatment.

Keywords: Hedgehog (Hh) pathway, Gli1 siRNA, gastric cancer stem cells, di-stearoyl-phosphatidyl-ethanolamine-hyaluronic acid (DSPE-HA) single-point conjugate, therapeutic siRNA nanoparticles

Introduction

Gastric cancer is the second leading cause of cancer-related death with 5-year overall survival rates of approximately 20% due to recurrence and metastasis, which are a major hallmark of failed clinical regimens.[1] Cancer stem cells (CSCs) are a pluripotent subpopulation of cells that may play a crucial role in therapeutic resistance, metastasis, and recurrence, as well as poor prognosis for

survival, due to their self-renewal, differentiation, and highly aggressive proliferation.[2,3] Quiescent undifferentiated CSCs have the intrinsic ability to detoxify and localize within hypoxic niches, in addition to other mechanisms, which allows them to escape cancer treatments.[4] Hence, effective targeting of CSCs in gastrointestinal tumors is believed to be a promising therapeutic strategy.

It is crucial to identify effective therapeutic targets with clinical implications in gastrointestinal cancer therapy. Previous studies have reported that only CD44 positive (CD44+) cells are required to form neoplastic tumors with gastric CSC-like properties.[5–8] Recent reports have further indicated that CD44 expression in human gastric carcinoma specimens may serve as an independent prognostic indicator for tumor progression, metastasis, and patient survival.[9–11] Thus, the subpopulation of CD44+ cells may serve as a potential therapeutic target for gastric CSCs. Moreover, the polysaccharide hyaluronic acid (HA) has been identified as a specific ligand for the CD44 receptor and may be a potential molecular target for CD44-overexpressing tumors.[12] Similar to polyethylene glycol (PEG), the HA coating provides a hydrophilic shield that promotes extended circulation in the blood.[13] In the present study, we took advantage of a number of HA properties including its excellent biocompatibility, biodegradability, nontoxicity, and non-immunotoxicity, to design targeted moieties in gastric CSCs with CD44 overexpression.[14]

A number of studies have shown that activation of the Hedgehog (Hh) signaling pathway is essential for maintaining and regulating CSC stemness in a variety of tumors,[15–19] suggesting that a blockade of the Hh pathway may serve as a novel therapeutic strategy for the treatment of CSCs. In addition, the Hh signaling pathway is only aberrantly activated in cancers, especially CSCs.[20] Therefore, the inhibition of molecules within the Hh pathway may avoid side effects in normal adjacent tissues. The transcription factor glioma-associated oncogene homolog 1 (Gli1) is a functional downstream protein in Hh pathway, and plays a central role in cancer stemness while serving as a reliable indicator of abnormal activity.[21] Moreover, high expression of Gli1 is associated with drug resistance,[22–25] metastasis,[26] tumorigenicity[27] and poor prognosis, and indicates progressive stages of cancer.[28,29] Hence, blocking Gli1 with small interfering RNA (siRNAs) may prove to be an ideal strategy for cancer treatment. Nevertheless, due to the molecular weight and polyanionic nature of siRNAs, their clinical application as therapeutic agents continues to be impeded by considerable obstacles, including ribonuclease (RNase) degradation, poor membrane permeability, short serum half-life, and inefficient tissue distribution and intracellular localization.[30]

The application of therapeutic siRNAs must be further improved by the development of effective delivery systems.[31] Cationic liposomes serve as effective siRNA delivery systems, as they have the ability to better protect their contents, are efficient at gene silencing, and accumulate in tumors due to their enhanced permeability and retention (EPR) effects.[32] However, high positive surface charges in vivo may reduce biocompatibility and cause serious side effects. Therefore, we proposed that a DSPE-HA conjugate could be employed to modify cationic liposomes to efficiently increase their biocompatibility and targetability to CD44+ CSCs, while simultaneously prolonging their circulation time in the blood. In most past studies, phospholipids have been coupled to HA via the carboxylic groups of HA and amine groups of phospholipids, using carbodiimide chemistry, resulting in multipoint attachments.[33,34] To retain HA chain integrity, which is important for its affinity with CD44 receptors, we coupled the reductive end of HA to amine groups of DSPE using a reductive amination method. The resulting DSPE-HA conjugate has a single coupling point.

Herein, we describe the generation of a DSPE-HA single-point conjugate and multipoint conjugate, which is an intrinsically tailored ligand of the CD44 receptor and a remarkable biomarker of gastric CSCs. The DSPE-HA conjugate was modified on the surface of nanoparticles. Thus, the novel therapeutic HA-mediated CSC-targeting Gli1 siRNA nanoparticles were developed to specifically target gastric CSCs. After development, the nanoparticles were functionally characterized for bioactivity, including CSCs targetability, inhibitory effect, and efficacy in preventing recurrence and metastasis. The potential mechanisms of action were also investigated.

Materials and Methods

Drugs and Agents

The 1,2-dioleoyl-3-trimethylammonium-propane (DOTAP) chloride salt, di-oleoyl- phosphatidyl-ethanol-amine (DOPE), di-stearoyl-phosphatidyl-ethanolamine (DSPE), and cholesterol were purchased from Avanti Polar Lipids, Inc. (Alabaster, AL, USA). Hyaluronic acid (Mw17500Da) was purchased from Zhenjiang Dongyuan Biotech Co., Ltd.

(Zhenjiang, China). Chondroitin sulfate (CS) was purchased from Dalian Meilun Biotech Co., Ltd. (Liaoning, China) and protamine was obtained from Sigma-Aldrich (St. Louis, MO, USA). Dulbecco's Modified Eagle Medium (DMEM) and fetal bovine serum (FBS) were obtained from Gibco (Billings, MT, USA). Epidermal growth factor (EGF) and basic fibroblast growth factor (bFGF) were purchased from Sigma-Aldrich. B27 supplement was obtained from Invitrogen (New York, NY, USA). Cell counting kit-8 (CCK-8) was obtained from Dojindo Laboratories (Kumamoto, Japan). OPTI-MEM was obtained from Invitrogen. Anti-CD44-fluorescein isothiocyanate (FITC) antibody was purchased from BD Biosciences (Franklin Lakes, NJ, USA). Antibodies against Gli1 and α-actin were purchased from Cell Signaling Technology (Danvers, MA, USA). Gli1-specific siRNA (sense strand: 5′-GGC UCAGCUUGUGUGUAAUTT-3′; antisense strand: 5′-AUUACACACAAGCUGAGCCTT-3′, designated as Gli1 siRNA), negative control scramble siRNA (sense strand: 5′-UUCUCCGAACGUGUCACGUTT-3′; antisense strand: 5′-ACGUGACACGUUCGGAGAATT-3′, designated as NC siRNA), and fluorescein-labeled siRNA (5′ end of the sense strand, designated as FAM siRNA) were synthesized by GenePharma Co. Ltd. (Shanghai, China).

Synthesis of DSPE-HA Conjugate

For the synthesis of DSPE-HA single-point conjugate, DSPE can be coupled to HA with a single coupling point via the aldehydic groups of HA and amine groups of DSPE by the reductive amination reaction method.[35] Briefly, hyaluronic acid (HA) was activated with tetra-n-butylammoniumhydroxide (TBA). Then activated HA-TBA (10 μmol) and DSPE (50 μmol) were dissolved in dimethyl sulfoxide. After stirring for 2 h at 60°C, sodium triacetoxyborohydride ($NaBH(OAc)_3$, 100 μmol) was added dropwise. The mixture was stirred at 60°C for 72 h. After dialyzing with 0.01 mol/L HCl solution, DSPE-HA single-point conjugate was obtained. For the synthesis of DSPE-HA multipoint conjugate, DSPE can be coupled to HA with multipoint attachment via the carboxylic groups of HA and amine groups of DSPE by carbodiimide chemistry as previously described.[36,37] HA (100 μmol) was activated with EDC (200 μmol) and NHS (200 μmol) for 2 h, and then added to DSPE (500 μmol) solution dissolved in 10% tert-butanol containing 0.1 mol/L triethylamine. After stirring for 6 h at 50°C and a further 48 h at 25°C, DSPE-HA multipoint conjugate was obtained. The final products were then lyophilized. The obtained DSPE-HA conjugate was confirmed using Fourier-transform infrared spectrometer (FTIR, JASCO FT/IR-4200 type A, JASCO Co., Tokyo, Japan). The amount of DSPE lipid covalently coupled to HA was quantified using the spectrophotometric method, according to the previous report.[38] Specifically, DSPE formed a coordination compound with ammonium ferrothiocyanate for detection. Next, the content of DSPE was analyzed by spectrophotometric method and detected at 468 nm, followed by calculation for the molar ratio of DSPE to HA.

Preparation and Characterization of siRNA Nanoparticles

Targeting Gli1 siRNA nanoparticles were prepared using the layer-by-layer assembly method. First, to prepare cationic liposomes, DOTAP, DOPE and cholesterol with a molar ratio of 1:1:1 were dissolved in chloroform that was removed by rotary evaporation. The remaining film was hydrated in DEPC-treated ddH_2O, followed by probe sonication for 10 min at 120 W. Suspensions were filtered three times through membranes of pore sizes 400 and 200 nm to yield cationic liposomes. Second, siRNA and CS (1:1, mass ratio) were mixed, followed by the addition of an equal mass of protamine. The mixture was incubated for 10 min to obtain a protamine/CS/Gli1 siRNA nanocomplex. Third, the protamine/CS/Gli1 siRNA nanocomplex and cationic liposomes (lipid: siRNA, 1000: 1, molar ratio) were mixed for 10 min to obtain the Gli1 siRNA nanoparticles. Fourth, targeting Gli1 siRNA nanoparticles were prepared by incubating Gli1 siRNA nanoparticles with DSPE-HA single-point conjugate (lipid: DSPE-HA single-point conjugate, 100: 5, molar ratio) at 50°C for 10 min. For blank targeting nanoparticle carriers, the preparation process was the same as described above, except that siRNA was not added. For the preparation of FAM siRNA nanoparticles used for in vitro cellular uptake, and of Cy5.5 siRNA nanoparticles for the in vivo biodistribution experiment, the procedure was the same as described above. The particle sizes and zeta potentials of the prepared nanoparticles were determined using a Zetasizer Nano ZS90 instrument (Malvern Instruments Ltd., U.K.). Stability was evaluated by measuring the changes in mean particle size and relative turbidity in PBS containing 50% FBS.

Cell Culture and Gastric CSC Sorting

The human gastric cancer cell line AGS was obtained from the Shanghai Cell Bank of the Chinese Academy of

Medical Sciences (Shanghai, China) and cultured in DMEM medium supplemented with 10% FBS, 100 U/mL penicillin, and 100μg/mL streptomycin. Gastric CSCs were isolated by sorting CD44+ cell subpopulations using anti-CD44-FITC antibodies by fluorescence activated cell sorting (FACS). Thus, the tumor spheroid of gastric CSCs was cultured. Briefly, the CD44 + subpopulation was sorted from AGS cells, seeded into ultralow attachment six-well plates (Corning, Lowell, MA, USA), and cultured in stem cell medium (serum-free DMEM medium supplemented with 20 ng/mL EGF, 10 ng/mL bFGF, 1% B27 supplement, 100 U/mL penicillin, and 100 μg/mL streptomycin). Cells were cultured in a humidified incubator at 5% CO_2 and at 37°C.

Immunofluorescence Analysis

Immunofluorescence analysis was used to evaluate Gli1 expression in CD44+ cells and CD44− cells. Briefly, the CD44+ cells and CD44− cells were fixed with 4% paraformaldehyde and permeabilized with 0.5% Triton X-100. Then, the cells were blocked with 1% BSA and incubated with Gli1 antibodies at 4°C overnight. After incubating with Alexa Fluor-conjugated secondary antibodies and 5 μg/mL 4′, 6- diamidino-2-phenylindole (DAPI) for 30 min, the cells were observed using a laser scanning confocal microscope.

Enzyme-Linked Immunosorbent Assay (ELISA)

ELISA assay was performed to measure the binding affinity of the DSPE-HA single-point conjugate and multipoint conjugate with the CD44 receptor, according to the manufacturer's protocol (Tiangen, Beijing, China). Briefly, the wells of microtiter plates were coated with HA, DSPE-HA single-point conjugate and multipoint conjugate at 4°C overnight, respectively. After being blocked with 2% BSA, CD44-IgG Fc fusion protein was added, and subsequently incubated for 1 h. Then, anti-human IgG Fc-HRP was added, followed by incubation for 1 h. Subsequently, TMB was added, and absorbance intensity was determined at 450 nm.

Flow Cytometry Analysis

The intracellular targeting efficiency of the nanoparticles was investigated by flow cytometry using FAM siRNA as a fluorescent probe. Briefly, CD44+ cells were seeded into six-well plates and incubated for 24 h. After incubation with various FAM siRNA formulations, the cells were harvested and examined using the FACScan flow cytometer. For competition experiments, the cells were pre-incubated with excess free HA (5 mg/mL) for 30 min to saturate the CD44 receptors. The targeting FAM siRNA nanoparticles were then added as detailed above.

Confocal Microscopy Analysis

Qualitative analysis was performed using confocal microscopy. The CD44+ cells were cultured in glass-based dishes and were incubated for 24 h to allow attachment. The cells were then incubated with various FAM siRNA formulations as described above. After incubation for 3 h, the cells were washed and fixed with 4% paraformaldehyde (v/v). Cell nuclei were then stained with DAPI (5 μg/mL). Finally, the cells were washed and examined using a Leica SP2 confocal microscope (Leica, Heidelberg, Germany).

Western Blot Analysis

For in vitro evaluation of gene silencing, CD44+ cells were treated with various formulations containing 200 nM Gli1 siRNA or NC siRNA in OPTI-MEM medium. After 6 h of incubation, the supernatant was removed and the cells were incubated with fresh complete culture medium for 36 h. Cells were collected and cell lysates were used for Western blot analysis. Antibodies against Gli1 and α-actin (Cell Signaling Technology) were used.

Cell Proliferation and Apoptosis Assay

To evaluate the inhibitory effects of the various nanoparticles on gastric CSCs, CD44+ cells seeded in 96-well plates were exposed to a series of concentrations of the various nanoparticles in OPTI-MEM for 48 h at 37°C. Their antiproliferative activity was measured using CCK-8 assays, according to the manufacturer's protocols. The morphological changes and ultrastructure of CD44+ cells treated with the various nanoparticles were investigated by atomic force microscopy (AFM, JPK NanoWizardI, Germany).

Colony Formation Inhibition Assay

CD44+ cells were treated with the various nanoparticles containing 100 nM Gli1 siRNA for 6 h. The supernatant was then replaced with fresh culture medium and changed every three days. After incubated for 10 d, the cells were fixed with methanol for 15 min at 25°C and visualized by staining with 1% methylene blue.

Tumor Spheroid-Formation Assays

Inhibition of tumor spheroid-formation by CD44+ cells following treatment with various Gli1 siRNA formulations

was determined using the tumor spheroid culture technique. Briefly, CD44+ cells were seeded into ultralow attachment six-well plates in stem cell medium and treated with the various nanoparticles at 37°C for 7 d. The numbers of spheroids formed were counted as observed using a phase-contrast microscope.

Soft Agar Colony Formation Assays

Inhibition of colony formation by CD44+ cells following treatment with the various Gli1 siRNA formulations was measured using soft agar assays. The assays were performed using 0.6% and 0.3% soft agar in DMEM supplemented with 10% FBS, as the base and top layers, respectively. The cells were treated with the various nanoparticles at 37°C for 14 d. Colony formation was visualized and photographed using a phase-contrast microscope.

Wound-Healing Assay

Wound-healing migration assays were used to evaluate the horizontal movement of CD44+ cells. Briefly, CD44+ cells were treated for 6 h with the various nanoparticles. After the supernatant was replaced with fresh complete culture medium, a single scratch wound in the confluent cells was created using a sterile micropipette tip. After washing with PBS, the remaining cells were cultured for 24 h. The width of the scratch was viewed using a phase-contrast microscope at 0 h and 24 h post wounding. Original and migration areas were measured using ImageJ software.

Cell Migration and Invasion Assay

Cell migration and invasion were detected using Transwell chambers. For the migration assay, cells treated with various siRNA nanoparticles containing 100 nM siRNA were seeded into the upper chamber in serum-free medium. The lower chamber contained DMEM plus 10% FBS. After 24 h incubation, the migrated cells were stained with Giemsa stain and were counted under a light microscope. For the invasion assays, the procedures were the same, except that Matrigel (BD Bioscience) was added to the upper chamber.

3D Tumor Spheroids Penetration Assays

The CD44+ cell spheroids were transferred to the 48-well culture plate at one spheroid per well. To observe the penetration ability, the spheroids were incubated with targeting FAM siRNA nanoparticles and were scanned at the different layers using a confocal laser scanning fluorescence microscope. To evaluate the growth-inhibitory effect, the spheroids were treated with the various nanoparticles, and their maximum diameter (d_{max}) and minimum diameter (d_{min}) were measured under an inverted microscope. Spheroid volume was calculated using the formula $V= (\pi \times d_{max} \times d_{min})/6$. The volume–change ratio of spheroids was obtained using the formula $R\ (\%) = (V_{dayi}/V_{day\ 0}) \times 100$, where $V_{day\ i}$ is the spheroid volume of at the i^{th} day (day 1, 2, 3, 4, or 5) after treatment with nanoparticles, and $V_{day\ 0}$ is the spheroid volume before treatment. The morphological changes of the spheroids at day 3 after treatment were viewed under a scanning electron microscope (SEM).

In vivo Imaging

Noninvasive optical imaging systems were used to evaluate the real-time distribution and tumor accumulation of Cy5.5-labeled siRNA nanoparticles in BALB/c nude mice bearing AGS-derived CSC xenografts. The male mice (18–20 g) were purchased from the Chinese Academy of Medical Sciences Institute of Zoology. When the tumor volumes reached approximately 500 mm^3, the mice were treated with Cy5.5-labeled siRNA nanoparticles and scanned using IVIS 200 imaging system (Xenogen Co., Alameda, CA, USA). After in vivo imaging 24 h post-treatment, the mice were sacrificed by cervical dislocation and the tumors and major organs were excised, and photographed.

Evaluation of Relapsed Tumor Growth

Approximately 8×10^4 CD44+ gastric CSCs were subcutaneously injected into the right flanks of five-week-old BALB/c nude mice obtained from the Institute of Zoology, Chinese Academy of Medical Sciences, Beijing, China. When the tumors reached 150–180 mm^3 in volume, the mice were treated with various nanoparticles. Mice were monitored daily for tumor progression and weight changes.

Animal protocols were approved by the Institutional Animal Care and Use Committee of the Institute of Medicinal Biotechnology, Chinese Academy of Medical Sciences & Peking Union Medical College. The use of experimental mice was in accordance with policies regarding the welfare of laboratory animals, according to the guidelines of the Ethical Examination Form of Laboratory Animals and Working System of Laboratory Animal Room, based on the Regulations on Ethical Review of Laboratory Animals in the Institute of Medicinal Biotechnology.

Statistics Analysis

Data are presented as the mean ± standard deviation using SPSS software. One-way analysis of variance (ANOVA) was used to determine the significance of the differences among groups, after which post hoc tests with Bonferroni correction were used to compare individual groups. A p-value <0.05 was considered statistically significant.

Results

Synthesis and Representation of DSPE-HA Conjugates

Figure 1A and B illustrates the synthesis routes of DSPE-HA single-point and multipoint conjugate, respectively. Specifically, to synthesize DSPE-HA single-point conjugate, HA was conjugated with DSPE by reductive amination between the aldehydic groups of HA at the reducing end and amine groups of DSPE, using $NaBH(OAc)_3$ as the reducing agent. DSPE-HA multipoint conjugate was generated by carbodiimide chemistry in which carboxylic acid groups of HA activated by NHS and EDC were coupled to amine groups of DSPE. Next, both of the DSPE-HA conjugates were characterized. As shown in Figure 1C, HA had a broad stretching band in the region of 3200–3600 cm^{-1} related to hydroxyl groups, and a sharp peak at 1617 cm^{-1} due to its carboxylic groups. The DSPE spectrum showed sharp absorbance peaks at 1742 cm^{-1} and at 2850–2918 cm^{-1}, indicating carbonyl and methylene groups in the acyl chains, respectively. Moreover, DSPE showed a broad stretching band at 3425 cm^{-1} related to the amine group. We found that the spectrum of either single- or multiple-point DSPE-HA conjugate showed a peak at 2850–2918 cm^{-1} related to methylene groups, together with a sharp absorbance peak at 1742 cm^{-1} representing carbonyl in the acyl chains of DSPE. There was also a broadband at 3406 cm^{-1}, implying hydroxyl groups of HA.

These results suggest that the chemical structure of the DSPE-HA conjugate has hydroxyl groups of HA, methylene groups, and carbonyl groups of DSPE, confirming the successful coupling between DSPE and HA. However, the spectrum of the DSPE-HA single-point conjugate showed a sharp peak at 1617 cm^{-1} related to the carboxylic groups of HA (Figure 1C), suggesting that the single-point conjugate retained the integrity of the HA chain. In contrast, the peak intensity of carboxyl groups was significantly lower for the DSPE-HA multipoint conjugate than for the single-point conjugate. This implies that the DSPE-HA single-point conjugate was successfully synthesized, but not through reactions with the carboxylic groups of HA chains. The quantitative lipid assay revealed molar ratios of DSPE linked to HA of 8.89:1 (DSPE-HA multipoint conjugates) and 0.82:1 (DSPE-HA single-point conjugates).

Synthesis and Representation of siRNA Nanoparticles

Subsequently, we generated targeting Gli1 siRNA nanoparticles by inserting DSPE-HA conjugates (Figure 2A), followed by an analysis of biophysical features. Specifically, the sizes of different particles, including protamine/CS/Gli1 siRNA complexes, cationic liposomes, Gli1 siRNA nanoparticles, and targeting Gli1 siRNA nanoparticles were determined to be 101 nm, 109 nm, 123 nm, and 127 nm, respectively (Figure 2B). As shown in Figure 2C, the zeta potential of the protamine/CS/Gli1 siRNA complexes was approximately −20 mV, due to the relative excess of negatively charged components. After the addition of cationic liposomes, the zeta potential of the resultant nanoparticles increased to approximately +35 mV. Insertion of DSPE-HA conjugates induced a reduction in zeta potential from +35 mV to −14 mV, suggesting the successful wrapping of HA onto the surface of Gli1 siRNA nanoparticles via layer-by-layer electrostatic interactions. The change in zeta potentials illustrates the systematic formation process of targeting Gli1 siRNA nanoparticles. For comparison, non-targeted Gli1 siRNA nanoparticles were constructed, in which DSPE-PEG was inserted instead of DSPE-HA. Other cargo-loaded targeting nanoparticles, including FAM siRNA and Cy5.5-siRNA, had similar sizes and zeta potentials as the Gli1 siRNA loaded targeting nanoparticles. This suggests the stability of the DSPE-HA modified targeting nanoparticles.

To determine whether the DSPE-HA coating would improve nanoparticle stability, the changes over time in particle sizes of Gli1 siRNA nanoparticles and targeting Gli1 siRNA nanoparticles were monitored in the presence of 50% FBS. As shown in Figure 2D, the mean diameter of Gli1 siRNA nanoparticles immediately increased from approximately 120 nm to 500 nm upon addition of the FBS. Over time, the particle sizes continued to increase to approximately 1100 nm at 24 h. However, targeting Gli1 siRNA nanoparticles, which were approximately 120 nm, exhibited almost no change in particle size. Furthermore,

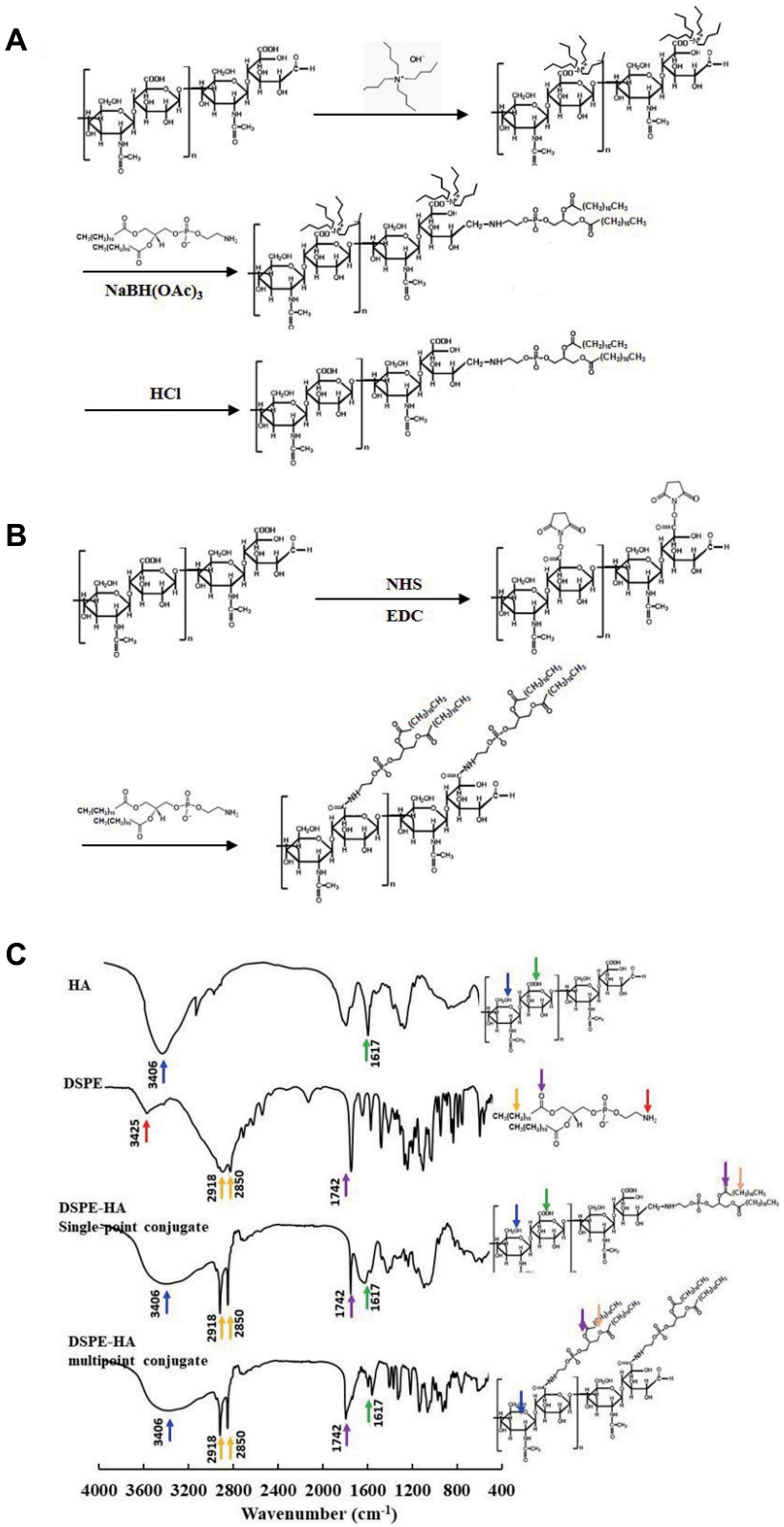

Figure 1 Synthesis and representation of di-stearoyl-phosphatidyl-ethanolamine- hyaluronic-acid (DSPE-HA) conjugate. (**A**) Synthetic scheme for DSPE-HA single-point conjugate. (**B**) Synthetic scheme for DSPE-HA multipoint conjugate. (**C**) Fourier transform infrared (FTIR) spectra of HA, DSPE, and DSPE-HA single-/multiple-point conjugate.

Notes: Blue arrows: hydroxyl groups of HA; Green arrows: carboxylic groups of HA; Red arrows: amine groups of DSPE; Orange arrows: methylene groups of DSPE; Purple arrows: carbonyl groups of DSPE.

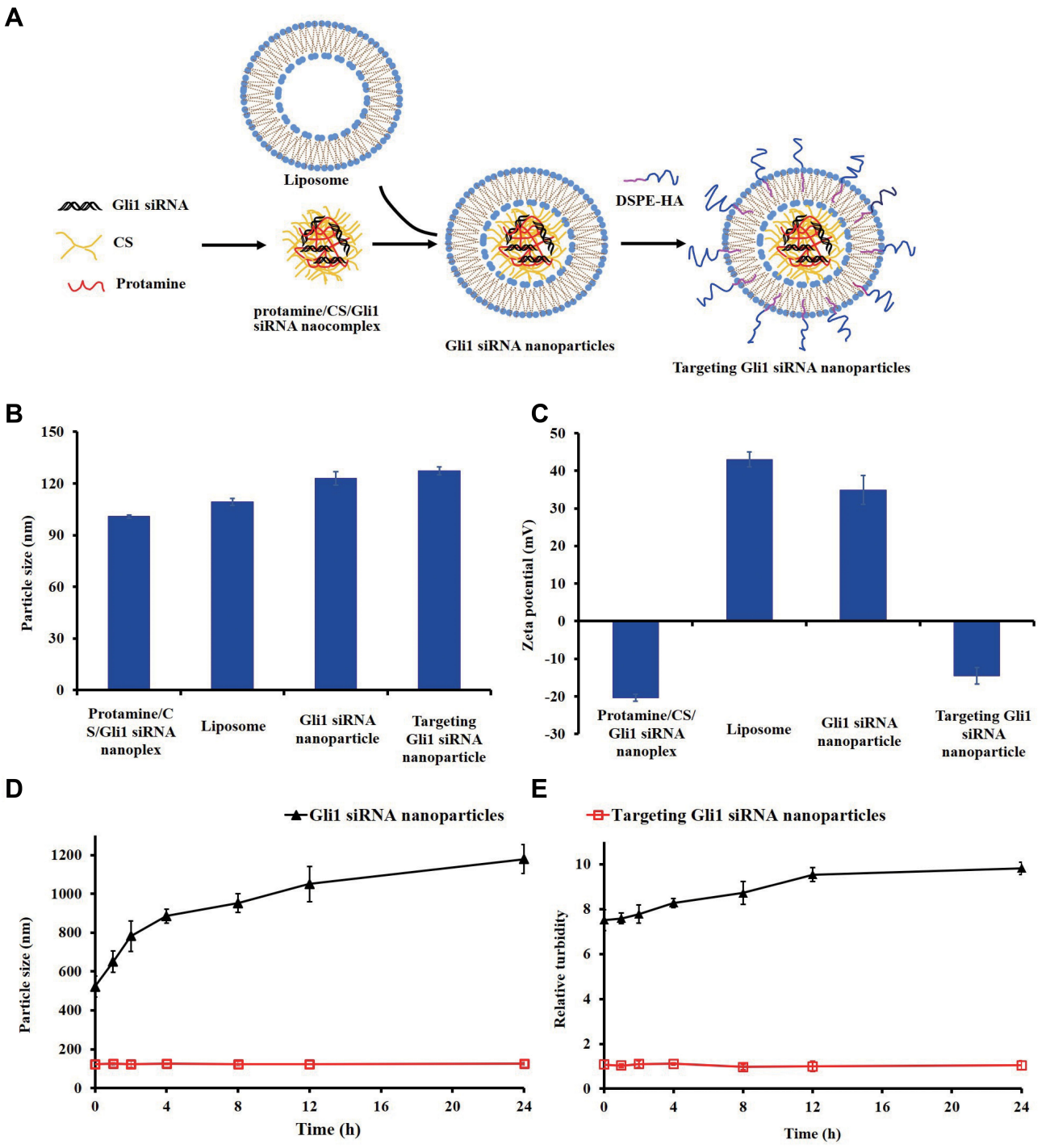

Figure 2 Preparation and representation of targeting Gli1 siRNA nanoparticles. (**A**) Schematic illustration of the process for preparing targeting Gli1 siRNA nanoparticles. Cationic liposomes composed of 1,2-di-oleoyl-3-trimethyl-ammonium-propane (DOTAP), di-oleoyl-phosphatidyl- ethanol-amine (DOPE), and cholesterol were prepared by thin-film hydration followed by ultrasonic dispersion. Negatively charged nanoparticle cores were ternary electrostatic complexes composed of Gli1 siRNA, CS, and protamine. The cores were further encapsulated with cationic liposomes using a self-assembly technique to produce core-shell Gli1 siRNA nanoparticles. Targeting Gli1 siRNA nanoparticles were generated by insertion of DSPE-HA conjugates. The particle sizes (**B**) and zeta potentials (**C**) of protamine/chondroitin sulfate (CS)/Gli1 siRNA complexes, cationic liposomes, Gli1 siRNA nanoparticles, and targeting Gli1 siRNA nanoparticles. Particle size changes (**D**) and relative turbidity (**E**) of Gli1 siRNA nanoparticles and targeting Gli1 siRNA nanoparticles in 50% FBS. Data are presented as the mean ± SD (n = 3).
Abbreviation: CS, chondroitin sulfate.

changes in the relative turbidity of non-targeting and targeting Gli1 siRNA nanoparticles were in accordance with the size changes of each group (Figure 2E). These experiments demonstrated that targeting Gli1 siRNA nanoparticles exhibited better stability in FBS due to their anionic charge.

Identification of CD44 and Gli1 in Gastric CSCs

Because CD44 serves as a marker for identifying CSCs in gastric cancer,[5,39] we used the fluorescence-activated cell sorting (FACS) method to isolate CD44+ and CD44− cell subpopulations from AGS cells. The results show that the proportion of CD44+ cells in the gastric cancer AGS cells was 5.78% (Figure 3A). After 10 days of incubation, CD44+ cells showed spherical colony formation, while CD44− gastric cancer cells formed few or no colonies (Figure 3B). Over time, the purity of CD44+ cells dissociated from the tumor spheroids increased to approximately 96%, which was much higher than that of CD44− cells (Figure 3B).To distinguish the biological features of the sorted CD44+ and CD44- cells, we further tested their susceptibilities to antineoplastic agents, as illustrated in Figure 3C. CD44+ cells showed more significant resistance to 5-fluorouracil, mitomycin C, epirubicin and docetaxel, than CD44− cells. This illustrates that we successfully identified these sorted CD44+ cells as gastric CSCs. Furthermore, the results of the immunofluorescence assays demonstrated much higher expression levels of Gli1 in CD44+ than in CD44− cells (Figure 3D). These results allowed us to design therapeutic nanoparticles for dual-targeting CD44 and Gli1 in gastric CSCs.

Efficient Targeting of CD44+ and Gli1 in Gastric CSCs

Next, we compared the binding affinity to the CD44 receptor of the DSPE-HA single-point or multipoint conjugates, using HA as a positive control. As shown in Figure 4A, all three demonstrated significant binding to CD44 in a concentration-dependent manner. The DSPE-HA single-point conjugate showed a higher binding affinity than multipoint conjugate. There was no significant difference in binding affinity between the DSPE-HA single-point conjugate and HA across all concentrations. Consequently, the DSPE-HA single-point conjugate was chosen for the preparation of CSC-targeting Gli1 siRNA nanoparticles in follow-up studies, because of its greater binding affinity to the CD44 receptor.

To quantitatively investigate cellular uptake into CD44+ CSCs of free FAM siRNA, FAM siRNA nanoparticles, or targeting FAM siRNA nanoparticles, we performed flow cytometry to detect the fluorescence intensity of internalized FAM. As shown in Figure 4B, targeting FAM siRNA nanoparticles showed significantly higher levels of cellular uptake than non-targeting FAM siRNA nanoparticles. Moreover, in competitive binding assays (Figure 4B), excess free HA significantly inhibited the uptake of targeting FAM siRNA nanoparticles, via endocytosis mediated by the interaction of the HA ligand and CD44 receptor. Figure 4B suggests that the targeting FAM siRNA nanoparticles were selectively guided to and internalized into CD44+ CSCs via endocytosis.

Consistent with the results from flow cytometry (Figure 4B), we observed greater intracellular accumulation and specific distribution of targeting Gli1 siRNA nanoparticles under a confocal microscopy (Figure 4C), and reduced intensity when samples were pre-treated with free HA. We further evaluated the distribution of siRNA nanoparticles in time course (Figure 4D). When treated for 1 h, targeting FAM siRNA nanoparticles that were stained in extensive yellow were colocalized in lysosomes with very limited staining in green. However, the green staining in the cells gradually increased with a corresponding reduction in yellow staining, and disappeared nearly 8 h post-treatment, showing that most of the siRNA had escaped from the lysozymes.

As shown in Figure 4E, Gli1 protein levels in CD44+ CSCs treated by either non-targeting or targeting Gli1 siRNA nanoparticles were significantly down-regulated in Western blot assay. Blank and targeting NC siRNA nanoparticles had no effect on Gli1 protein expression. Furthermore, Gli1 expression in cells treated with targeting Gli1 siRNA nanoparticles showed a significantly stronger reduction than those treated with non-CSC targeting Gli1 siRNA nanoparticles, due to the enhanced efficiency of siRNA delivery via HA-CD44 mediated internalization.

Significant Inhibition of Gastric CSCs Stemness in vitro

After determining the selective endocytosis and specific inhibition of Gli1 expression by targeting Gli1 siRNA nanoparticles, we tested if they had an effect on the cellular proliferation of CD44+ CSCs. As shown in Figure 5A, blank targeting nanoparticles did not exhibit any obvious cytotoxicity even at the highest concentration, suggesting that targeting nanoparticles may serve as suitable vehicles for drug delivery without causing serious cytotoxicity. Moreover, targeting Gli1 siRNA nanoparticles significantly inhibited cell proliferation at different concentrations, stronger than that of non-CSC-targeting Gli1 siRNA nanoparticles. These results imply that Gli1 siRNAs were more readily internalized into CD44+ cells via HA ligand-mediated endocytosis, leading to significant increases in their delivery efficiency and greater inhibitory rate of cell proliferation.

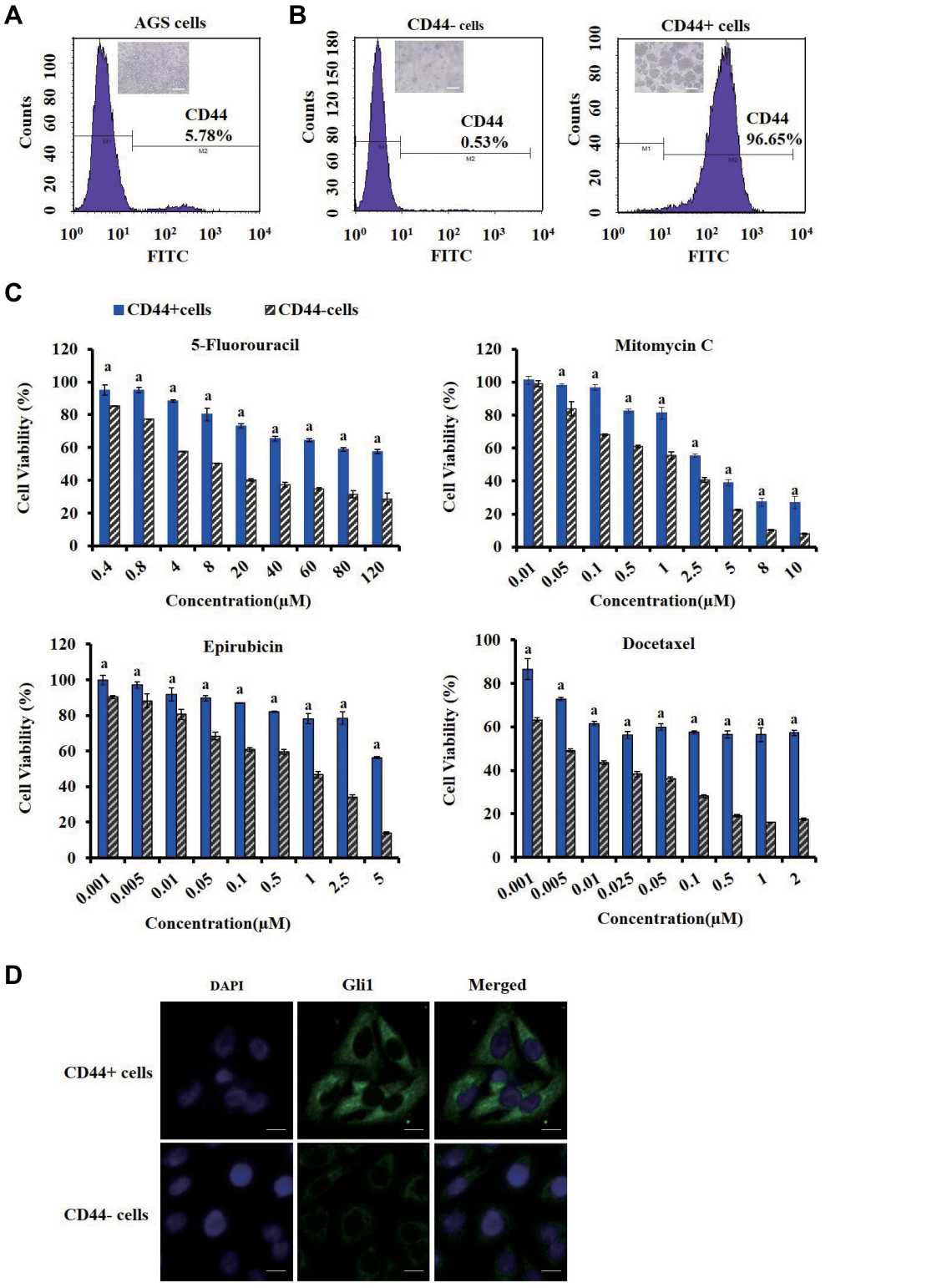

Figure 3 Identification of CD44 and Gli1 in gastric cancer stem cells (CSCs). (**A**) Expression of CD44 marker of AGS cells stained with FITC-conjugated CD44 antibody by fluorescence-activated cell sorting (FACS) analysis. (**B**) The purity of CD44+ and CD44− cells dissociated from the tumor spheroids in serum-free medium. Those cells were stained with FITC-conjugated CD44 antibody and subjected to flow cytometry analysis to determine the CD44 expression. (**C**) Comparison of chemo-resistance between CD44+ and CD44− cells. CD44+ and CD44− cells were exposed to a series of concentrations of 5-fluorouracil (0.4−120μM), mitomycin C (0.01−10μM), epirubicin (0.001−5μM) and docetaxel (0.001−2μM), respectively. The CCK-8 assay was performed at the end of incubation. (**D**) Immunofluorescence analysis of Gli1 in CD44+ and CD44− cells using laser scanning confocal microscopy. Cells fixed by paraformaldehyde were stained with anti-Gli1 antibodies followed by incubation with fluorescent secondary antibodies and DAPI staining of the nucleus. Green staining denotes the anti-Gli1 antibody and blue indicates the nuclei of CD44+ or CD44− cells. Scale bars indicate 20 μm.

Note: [a] Indicates $p < 0.05$ as compared with CD44− cells.

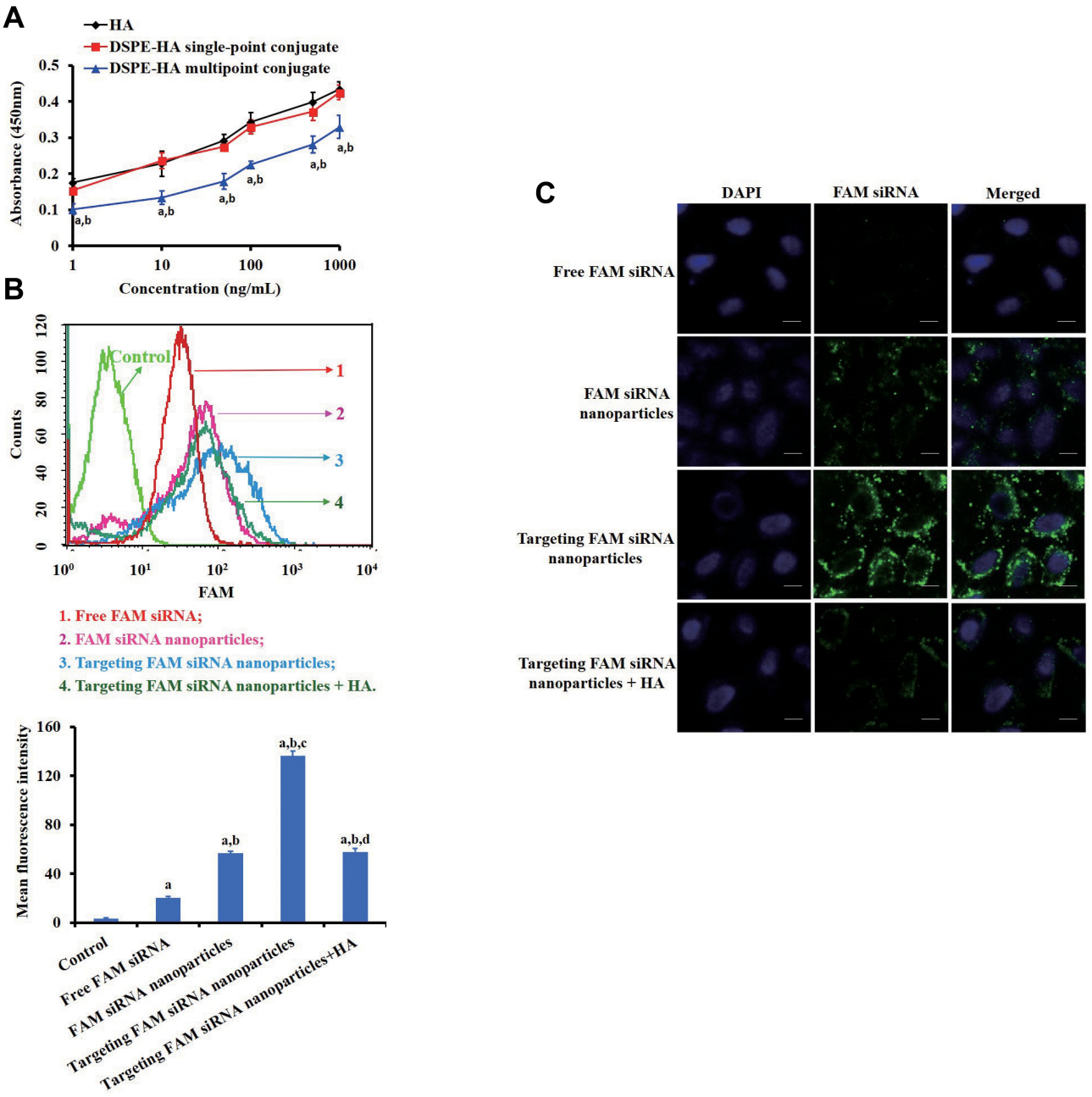

Figure 4 Continued.

We further assessed the effects of targeting Gli1 siRNA nanoparticles on CD44+ cells by AFM to examine the changes in cellular topography, ultrastructure, and morphology at the molecular level. As shown in Figure 5B, intact cell membranes, cytoskeletal fibers, and dense filopodia and lamellipodia were observed clearly in control cells, and in cells treated with targeting NC siRNA nanoparticles. After treated with Gli1 siRNA nanoparticles, the cells seemed to be contracted with some holes and truncated lamellipodia. However, cells incubated with targeting Gli1 siRNA nanoparticles appeared shrunken with nucleus fragmentation and partial structural collapse, as well as loss of filopodia and lamellipodia. This suggests that the targeting Gli1 siRNA nanoparticles exhibited much stronger inhibitory effects than Gli1 siRNA nanoparticles.

Subsequently, we investigated the effects on CSC self-renewal of targeting Gli1 siRNA nanoparticles by using colony, tumor spheroid, and soft agar colony formation assays. The results in Figure 5C revealed that targeting Gli1 siRNA nanoparticles more significantly inhibited plate

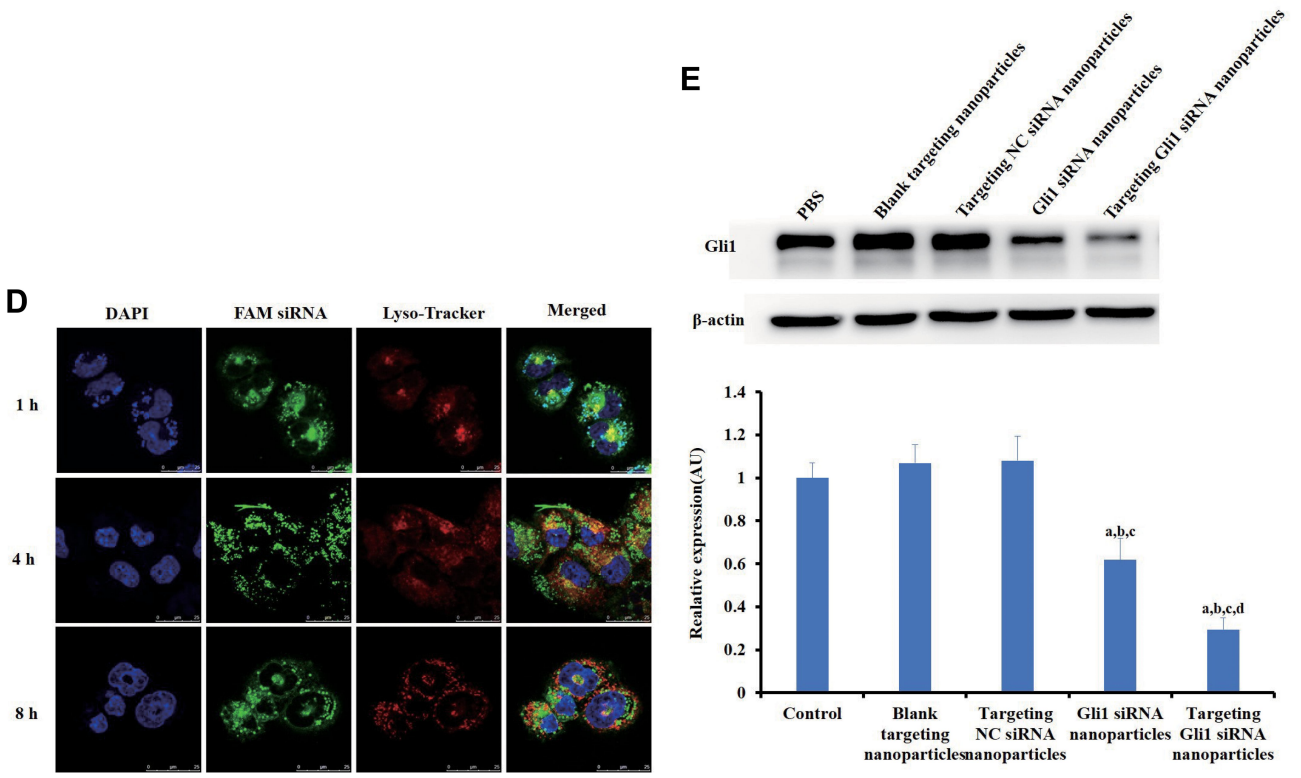

Figure 4 Effects of targeting CD44+ and Gli1 in gastric cancer stem cells (CSCs). (**A**) The binding affinity to recombinant human CD44 receptor of the di-stearoyl-phosphatidyl-ethanolamine-hyaluronic-acid (DSPE-HA) single-point and multipoint conjugates, analyzed by enzyme-linked immunosorbent assay (ELISA). Error bars indicate SD for n = 3. (**B**) A competitive binding assay was used to determine cellular uptake in CD44+ cells after treatment with either non-targeting or targeting FAM siRNA nanoparticles, with and without HA preincubation. After the culture medium was replaced by fresh OPTI-MEM, the cells were incubated with various formulations containing 100 nM FAM siRNA for 3h. The assay was analyzed using flow cytometry. The upper and lower panels show the images of flow cytometry analyses and quantitative evaluation of the mean fluorescent intensities, respectively. (**C**) Intracellular accumulation of siRNAs in CD44+ cells was investigated by laser scanning confocal microscopy analysis. The CD44+ cells were treated with free FAM siRNA, FAM siRNA nanoparticles, targeting FAM siRNA nanoparticles, or pre-treated with HA for 30 min followed by treatment with targeting FAM siRNA nanoparticles. Blue staining indicates the nuclei of CD44+ cells stained with DAPI while green indicates FAM siRNA. All data shown are representative of three independent experiments. a, b, c, and d: $p < 0.05$, compared with the control, free FAM siRNA, FAM siRNA nanoparticles, and targeting FAM siRNA nanoparticles, respectively. Scale bars indicate 20 μm. (**D**) Localization and distribution of targeting FAM siRNA nanoparticles in CD44+ cells. Lysosomes were visualized as red fluorescence due to staining of the cells with Lyso-Tracker Red DND-99; targeting FAM siRNA nanoparticles were visualized as green fluorescence. Blue indicates nuclei stained with Hoechst 33342. The red and green staining indicates non-colocalization of nanoparticles and lysosomes while yellow demonstrates colocalization of nanoparticles with lysosomes. Scale bars indicate 25 μm. (**E**) Gli1 expression levels in CD44+ cells treated with different Gli1 siRNA formulations were determined by Western blot analysis. Band intensities were quantified using ImageJ software. Data are presented as the mean ± SD (n = 3).
Notes: [a,b]Indicate $p < 0.05$ as compared with the HA and DSPE-HA single-point conjugate, respectively. [a-d]Indicate $p < 0.05$ as compared with the control, blank targeting nanoparticles, targeting NC siRNA nanoparticles, and Gli1 siRNA nanoparticles, respectively.

colony formation than Gli1 siRNA nanoparticles, whereas both blank and targeting NC siRNA nanoparticles had almost no effect on colony formation. Similar to the effects on CSCs colony formation, targeting Gli1 siRNA nanoparticles almost completely inhibited the capacity to form tumor spheroids (Figure 5D) and soft agar colony formation (Figure 5E). These results indicate that targeting Gli1 siRNA nanoparticles effectively inhibited the self-renewal capacity of CSCs.

Besides the above assays, we evaluated the malignant behavior of gastric CSCs with the treatment of targeting Gli1 siRNA nanoparticles by testing parameters of wound-healing, migration and Matrigel invasion. As shown in Figure 6A, the wound-healing rate in control cells at 24 h was 63.1%. Blank targeting nanoparticles and targeting NC siRNA nanoparticles had no effect on the rate. Gli1 siRNA nanoparticles reduced the wound-healing rate to 24.9%. However, the wound-healing response of CSCs was almost completely inhibited, with a wound-healing rate of 8.4% when samples were treated with targeting Gli1 siRNA nanoparticles. Subsequently, we evaluated the migration of CD44+ CSCs as shown in Figure 6B. The Gli1 siRNA nanoparticles significantly inhibited cell migration. Similarly, a greater inhibitory effect on invasion was observed (Figure 6C).

Effective Inhibition of 3D Tumor Growth via Effective Penetration

To evaluate the effect on tumor penetration of targeting Gli1 siRNA nanoparticles, we selected a 3D spheroid

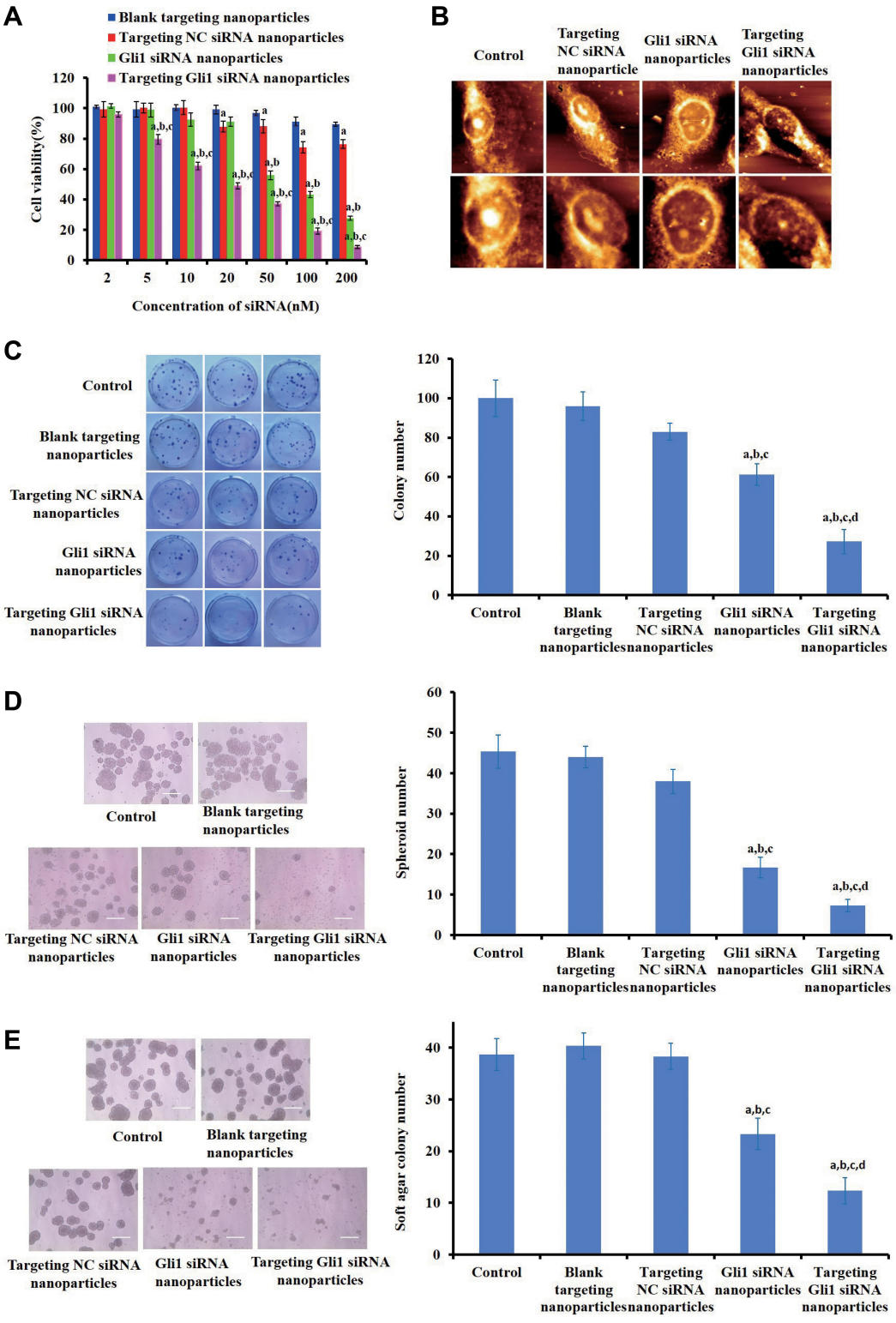

Figure 5 Influence on gastric cancer stem cell (CSC) stemness of targeting Gli1siRNA nanoparticles in vitro. (**A**) Effects of targeting Gli1 siRNA nanoparticles on cellular proliferation of CSCs based on CCK-8 assays. Data are presented as the mean ± SD from three independent experiments. a, b and c indicate $p < 0.05$ as compared with blank targeting nanoparticles, targeting NC siRNA nanoparticles, and Gli1 siRNA nanoparticles, respectively. (**B**) AFM images of CD44+ cells induced by PBS (pH 7.4), targeting NC siRNA nanoparticles, Gli1 siRNA nanoparticles and targeting Gli1 siRNA nanoparticles. The top and bottom images show full (60 × 60 μm^2) and magnified images (30 × 30 μm^2) of the cells, respectively. (**C–E**) Effects on CSC self-renewal of targeting Gli1 siRNA nanoparticles using colony (**C**), tumor spheroid (**D**) and soft agar colony (**E**) formation assays. Scale = 200 μm. The semi-quantification analysis for each experiment in (**C–E**) was performed as shown in bar graphs of the right panels, followed with a comparison test. Data are presented as the mean ± SD (n = 3).

Note: [a-d]Indicate $p < 0.05$ as compared with the control, blank targeting nanoparticles, targeting NC siRNA nanoparticles and Gli1 siRNA nanoparticles, respectively.

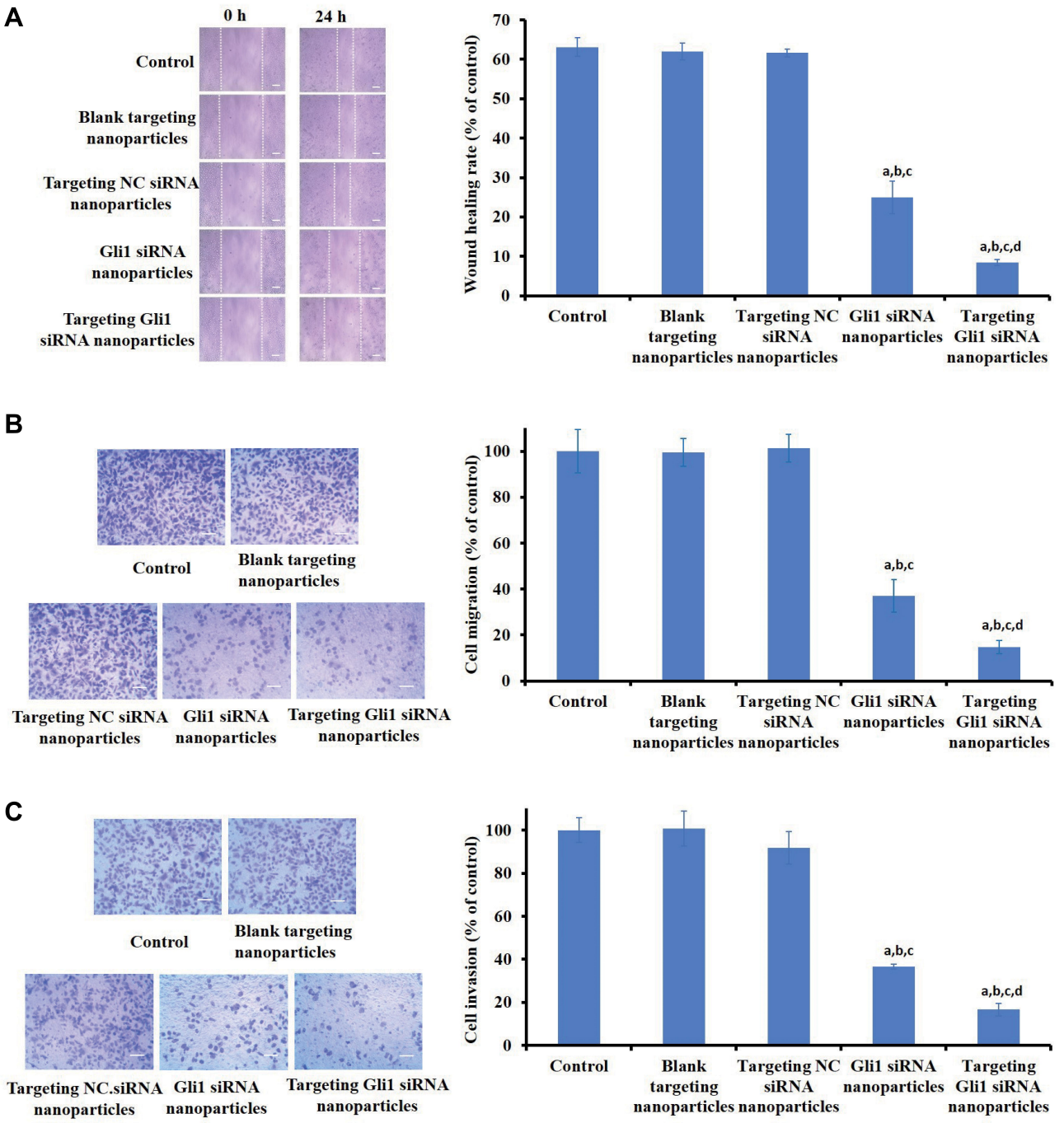

Figure 6 Effects on in vitro cell migration and invasion of targeting Gli1siRNA nanoparticles. (**A**) Wound-healing response of cancer stem cells (CSCs) to different Gli1 siRNA formulations detected using a wound-healing migration assays 24 h post-treatment. Invasive wounds of adherent CD44+ cells were created by single scratches in the cell monolayers using a pipettor tip. Wound-healing responses were subsequently evaluated for different Gli1 siRNA nanoparticle formulations at 0 h and 24 h post-treatment. The influence of different Gli1 siRNA formulations on CD44+ cell (**B**) migration capability based on cell migration assays and (**C**) invasion capability using Transwell Matrigel assays. The numbers of migrated and invaded cells from five random visual fields were determined from three independent experiments. The semi-quantification analysis for each experiment was performed as shown in a bar graph of the right panel, followed with comparison test.

Notes: [a-d]Indicate $p < 0.05$ as compared with the control, blank targeting nanoparticles, targeting NC siRNA nanoparticles, and Gli1 siRNA nanoparticles, respectively. Scale bar represents 100 μm.

model of gastric CSCs. Figure 7A shows the high well-penetration ability of targeting FAM siRNA nanoparticles into CSCs spheroids, with strong fluorescence in the range from −10 to −60 μm, whereas the cores of the spheroids treated with FAM siRNA nanoparticles were invisible (Figure 7B). Volumes of 3D spheroids treated with targeting Gli1 siRNA nanoparticles were obviously reduced compared with those treated with Gli1 siRNA

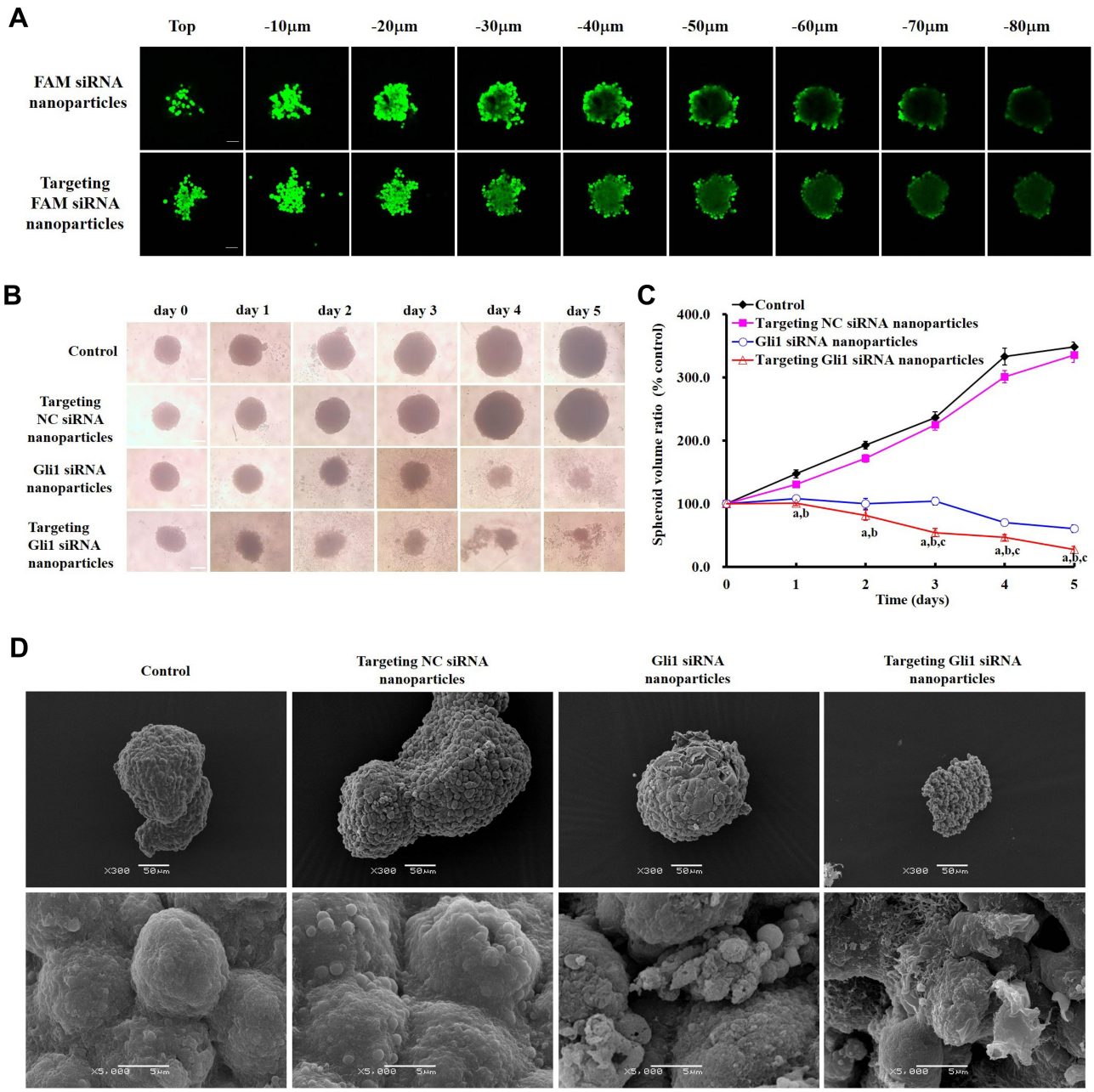

Figure 7 Effect on 3D tumor penetration and growth of cancer stem cells (CSC) spheroids. (**A**) Confocal images of CSC spheroids treated with FAM siRNA nanoparticles or targeting FAM siRNA nanoparticles for 12 h. Z-stack images were obtained from the top of the spheroid toward the equatorial plane in layers 10 μm thick. Scale bars indicate 40 μm. (**B**) The images of CSC spheroids treated with different nanoparticles under an inverted microscope. Scale bars indicate 200 μm. (**C**) Inhibitory effect on the growth of CSC spheroids after applying different nanoparticles. After treatment with the various nanoparticles, the maximum diameters (d_{max}) and minimum diameters (d_{min}) of the spheroids were measured under an inverted microscope. The spheroid volume was calculated using the following formula: $V= (\pi \times d_{max} \times d_{min})/6$. The volume-change ratio of spheroids was calculated using the formula $R= (V_{dayi}/V_{day\ 0}) \times 100\%$, where the $V_{day\ i}$ is the spheroid volume on the i^{th} day (Day 1, 2, 3, 4, 5) after treatment with nanoparticles, and $V_{day\ 0}$ is the spheroid volume before treatment. Data are presented as the mean ± SD (n =3). (**D**) Scanning electronic microscope (SEM) photographs of CSC spheroids after treatment with different nanoparticles at day 3. The images are shown at 300× and 5000 magnification, respectively.
Note: $^{a-c}$Indicate $p < 0.05$ as compared with the control, targeting NC siRNA nanoparticles and Gli1 siRNA nanoparticles, respectively.

nanoparticles. The ratios of spheroid volume change on Day 5 were 348.4 ± 7.2% for PBS, 335.4.5 ± 6.5% for targeting NC siRNA nanoparticles, 60.9 ± 8.3% for Gli1 siRNA nanoparticles and 27.3 ± 1.9% for targeting Gli1 siRNA nanoparticles (Figure 7C). Further, 3D spheroids via SEM images were detected in the groups treated with various nanoparticles on day 3 (Figure 7D). The spheroids treated with Gli1 siRNA nanoparticles had morphological changes with some sunkens compared to the controls. However, 3D spheroids after treated with

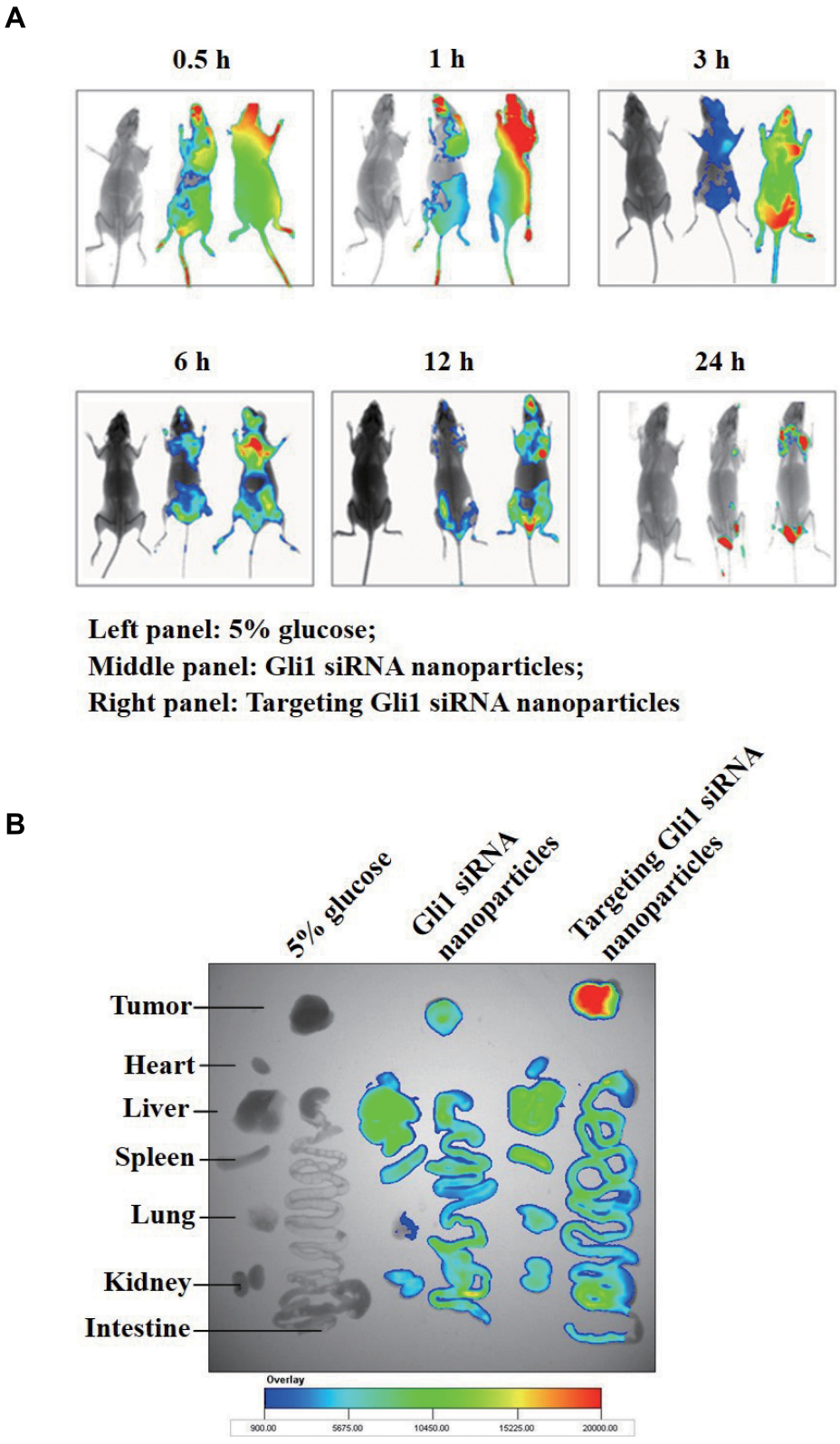

Figure 8 Specific in vivo distribution of Cy5.5-labeled siRNA in relapsed tumors (n = 3 mice/group). (**A**) In vivo imaging of relapsed tumors induced from AGS-derived gastric cancer stem cells (CSCs) in mice 0.5 h, 1 h, 3 h, 6 h, 12 h, and 24 h after intravenous injection of 5% glucose (left panel), Gli1 siRNA nanoparticles (middle panel), and targeting Gli1 siRNA nanoparticles (right panel). (**B**) Ex vivo optical images of tumors and organs of mice sacrificed after 24 h of treatment.

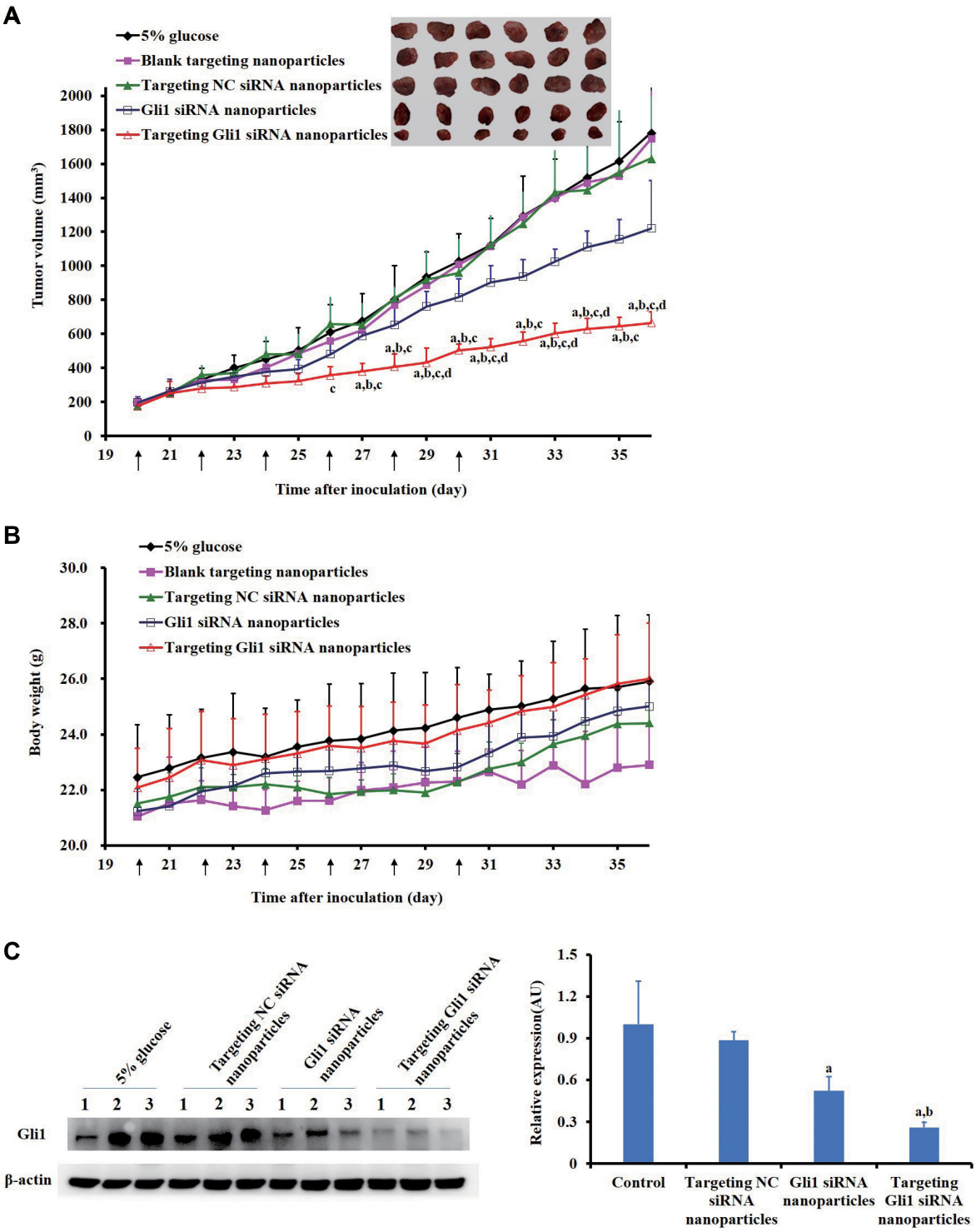

Figure 9 Efficacy of targeting Gli1 siRNA nanoparticles in BALB/c nude mice bearing relapsed tumors induced from AGS-derived cancer stem cells (CSCs). (**A**) Antitumor efficacy of treatments with 5% glucose, blank targeting nanoparticles, targeting NC siRNA nanoparticles, Gli1 siRNA nanoparticles, or targeting Gli1 siRNA nanoparticles. At 20 d, 22 d, 24 d, 26 d, 28 d, and 30 d post inoculation, the mice received, via tail vein injection, either 5% glucose, blank targeting nanoparticles, targeting NC siRNA nanoparticles, Gli1 siRNA nanoparticles, or targeting Gli1 siRNA nanoparticles at doses of 1 mg/kg siRNA. Data are presented as the mean ± SD (n = 6 mice/group). (**B**) Changes in body weight of mice bearing relapsed tumors after treatment with the agent indicated. The arrows under X-axis indicate the dates for treatments. (**C**) Protein levels of Gli1 expression in tumors after treatment were determined using Western blot assay. Three samples per group were analyzed. Protein band intensities were quantified by using Image J software. Data in the bar graph are the mean ± SD. Statistical significance was evaluated.

Notes: [a-d]Indicate $p < 0.05$ as compared with the treatment groups of 5% glucose, blank targeting nanoparticles, targeting NC siRNA nanoparticles, and Gli1 siRNA nanoparticles, respectively. The arrows under X-axis indicate the dates for treatments. [a,b]Indicate $p < 0.05$ as compared with the treatment groups of 5% glucose and targeting NC siRNA nanoparticles, respectively.

targeting Gli1 siRNA nanoparticles showed the most obvious morphological changes, including partial collapse, disintegration, and loss of 3D structure. This indicates that the targeting Gli1 siRNA nanoparticles effectively inhibited in vitro 3D tumor growth via effective penetration.

In vivo Imaging in Gastric Tumor Xenografts

To maximally enhance therapeutic effects and avoid toxicity, Cy5.5 fluorescent siRNAs were employed to track the biodistribution of the prepared nanoparticles by using in vivo imaging. As shown in Figure 8A and B, there was stronger fluorescence intensity in tumors treated with targeting Cy5.5 siRNA nanoparticles than in those treated with non-targeting nanoparticles. The results indicate the enhanced enrichment of fluorescence in tumors treated with targeting Cy5.5 siRNA nanoparticles, which might be attributed to the interaction of DSPE-HA conjugates with CD44.

Effective Repression of Relapsed Gastric CSC Tumors in vivo

To determine the in vivo efficacy of targeting Gli1 siRNA nanoparticles in CSCs, we established relapsed tumor models in BALB/c nude mice using a small number (8×10^4) of CD44+ CSCs sorted from the AGS cells that were used to generate new tumor masses according to a previous approach.[40] As shown in Figure 9A, tumor growth was significantly inhibited by targeting Gli1 siRNA nanoparticles. In contrast, treatment with blank targeting nanoparticles or targeting NC siRNA nanoparticles failed to inhibit tumor growth. No animals showed any significant changes in body weight (Figure 9B), suggesting a level of safety for this novel systemic siRNA delivery system. Significantly reduced levels of Gli1 protein in relapsed AGS tumor tissues treated with targeting Gli1 siRNA nanoparticles were further confirmed in Western blot analysis (Figure 9C), as compared to that in either untreated or NC siRNA nanoparticles treated groups.

Discussion

CSCs are responsible for metastasis, relapse, and chemoresistance or radio-resistance in cancer. Hence, the effective eradication of CSCs using novel therapeutic agents is of fundamental importance for curing and preventing relapse of gastric cancer. A myriad of signaling pathways have been described as being involved in CSC proliferation, self-renewal, differentiation and migration, such as Wnt, Notch and Hh.[41] Hh pathway is well known as an important signaling regulator in CSCs. It is initiated when Hh ligand binds to its receptor Patched (Ptch), resulting in inhibition of Smoothened (Smo) protein and subsequent activation of the downstream Gli proteins including Gli1, Gli2, and Gli3 as transcription factors (TFs). Gli1 activation, being the last essential step in the Hh signaling, plays a central role in CSC proliferation since it can be translocated into nucleus to regulate targeted gene expression.[42] Therefore, interventions targeting the Hh pathway via extracellular Hh ligands, membrane receptor Smo, and especially intracellular TF Gli proteins may be effective in eradicating CSCs, consequently reducing or preventing the recurrence and metastasis of cancer.[43] Therefore, in the present study, we developed a novel gene delivery system to inhibit Gli1 functioning in gastric CSCs using targeted nanoparticles with a self-assembly method. Since we had previously identified CD44 as a cell surface marker of gastric CSCs,[44] we successfully sorted and used CD44+ cells as gastric CSCs for the follow-up study to characterize our therapeutic siRNA nanoparticles (Figure 3A and B). We also demonstrated that Gli1 was more highly activated in these CD44+ cells than in CD44− cells (Figure 3D). That allowed us to design therapeutic nanoparticles for dual-targeting CD44 and Gli1 in gastric CSCs.

Previous analysis of the X-ray crystal structure of the HA-CD44 complex has indicated that oxygen atoms of the carboxylic groups in HA are associated with Gln24, Ala102, Ala103 and Tyr83, which play a key role in the recognition of CD44.[45] Computational simulations have also revealed that the carboxylic groups of HA were important to successfully achieve an interaction between HA and CD44.[45] Any chemical modification of carboxyl groups in HA would reduce its affinity. In the multipoint conjugates, carboxyl groups of HA were coupled with amine groups of DSPE, thus reducing its affinity with CD44 receptors. However, the coupling reaction for the DSPE-HA single-point conjugate occurred only in the aldehyde group at the reducing end of HA, which facilitated the conjugate to maintain the integrity of the whole carboxyl chain and gave it an excellent affinity with CD44 receptors. Therefore, in the present study, we designed to prepare for DSPE-HA single-point conjugate with a higher binding affinity than the multipoint conjugate for the first time (Figures 1, 2 and 4A).

To achieve systemic delivery of siRNA, one of the common strategies is to directly incorporate negatively charged siRNA with cationic liposomes by electrostatic interaction, in which siRNA is incorporated onto the surface of liposomes. However, there are a few disadvantages to this strategy. First, because siRNA is not readily condensed by cationic liposomes via electrostatic interaction, due to its rod-like rigidity, it tends to form looser complexes with cationic liposomes, which might cause low loading capacity, leading to potential leakage of the drug. Second, in terms of systemic administration, siRNA presented on the surface of the liposomes is subject to degradation in the enzyme-rich environment, or to replacement by negatively charged molecules, which shortens the effective circulating time of the delivery system. Third, common methods of surface decoration, such as PEGylation, may shield the positive charges of cationic liposomes or induce stereospecific blockades, and consequently impede the complexation of siRNA. Therefore, to solve the above problems and avoid using encapsulation of free siRNA in liposomes in the present study, we developed core-shell nanoparticles where the siRNA is encapsulated together with protamine and CS.

The zeta potential and particle size of the protamine/CS/Gli1 siRNA complexes changed according to the ratio of siRNA/CS to protamine. Once the ratio of siRNA/CS to protamine in the complex increased, the zeta potential decreased from positive to negative. The zeta potential of protamine/CS/siRNA complexes was about −20 mV, which is mainly due to the relative excess of negatively charged components of CS. In the present study, we chose 1.0 as the optimal ratio of siRNA/CS to protamine, because the complexes stayed negatively charged (−20 mV) with a relatively small size (~100 nm). These features facilitated compression and encapsulation with cationic liposomes via charge−charge interactions, to produce core-shell Gli1 siRNA nanoparticles.

We found that the particle sizes (127 nm) and zeta potential (−14 mV) of the targeting Gli1 siRNA nanoparticles (Figure 2B and C) effectively facilitated their stability, intracellular uptake, and targetability. First, we demonstrated in vitro stability of the targeting Gli1 siRNA nanoparticles which retained their properties for an extended time (Figure 2D and E) due to their anionic charge caused by DSPE-HA on their surface. Second, DSPE-HA single-point conjugate modified cationic liposomes were responsible for the enhancement of cellular uptake efficiency of the targeting FAM siRNA nanoparticles, via a CD44-mediated cellular uptake pathway. Our findings (Figure 4B and C) quantitatively and qualitatively confirmed that the targeting FAM siRNA nanoparticles were selectively guided to CD44+ gastric CSCs, followed by internalization via CD44 receptor-mediated endocytosis. Third, after internalization into the CD44+ cells, the targeting FAM siRNA nanoparticles became entrapped within endosomes or lysosomes. They may subsequently escape from the endosome or lysosome; otherwise, the siRNAs become degraded or leak out from the cells. To determine if the targeting FAM siRNA nanoparticles were able to escape lysosomal degradation following internalization, we evaluated their cellular distribution using confocal microscopy. Most of the siRNA was detected in lysosomes after 1 h of treatment with the targeting FAM siRNA nanoparticles; however, after 8 h, a large proportion of the nanoparticles were observed in the cytoplasm and at the periphery of the nucleus (Figure 4D). This confirmed that the siRNA successfully escaped lysosomal degradation after internalization. These results imply that after reaching the lysosomes, the FAM siRNA dissociated from the targeting FAM siRNA nanoparticles to function in the cytoplasm. This may be attributed either to the membrane disruption properties of cationic carriers or to the proton sponge effect of DOPE that was employed in the delivery system, as mentioned before.[46,47] This effect allowed our siRNAs to be released into the cytoplasm where they effectively silenced the gene expression of the target cells (Figure 4E).

In addition, to determine if the targeting nanoparticles enable efficient delivery of Gli1 siRNAs to CD44+ tumors, and accumulation of Gli1 siRNAs in these tumors, we performed in vivo imaging analysis to evaluate the distribution of siRNA in relapsed tumors derived from AGS-CSCs. Since Gli1 siRNA does not exhibit spontaneous fluorescence, we used fluorescent Cy5.5 siRNA as a probe and encapsulated it into targeting nanoparticles, as a surrogate for tracking the distribution of Gli1 siRNA. The results showed a clear increase in tumoral accumulation of targeting Cy5.5 siRNA nanoparticles, whereas non-targeted Cy5.5 siRNA nanoparticles were less stable (Figure 8A). We speculate that the targeting Cy5.5 siRNA nanoparticles remained in the tumor masses owing to extended circulatory and EPR effects. This was attributed to the modification of DSPE-HA forming a hydrophilic layer, leading not only to improved serum stability but also to prolonged residence in the systemic circulation. Besides the EPR effect,[48] the specific delivery

system via the ligand (HA)-receptor (CD44)-mediated interaction facilitated the increased enrichment in tumor tissue. Therefore, the HA motif enabled the targeting siRNAs to avoid rapid uptake by the reticuloendothelial system. However, the lower stability of non-targeted Cy5.5 siRNA nanoparticles may be attributed to their encountering and binding with a variety of plasma proteins, due to their high positive charge, because of faster clearance by the reticuloendothelial system in blood. In the present study, compared to non-targeted siRNA nanoparticles, our targeting siRNA nanoparticles had better accumulation capability in tumor. This novel delivery system, in which DSPE-HA single-point conjugates facilitate the specific and stable deposition of Gli1 siRNA in the tumor mass, was designed to improve both in vitro and in vivo tumor growth-inhibition by the targeting Gli1 siRNA nanoparticles.

Indeed, our bioactivity assays successfully demonstrated that the targeting Gli1 siRNA nanoparticles were able to interfere with gastric cancer relapse in vitro by inhibiting the stemness of gastric CSCs, as well as the growth of in vivo relapsed tumors (Figures 5, 6 and 9). In addition, our CSC-targeted approach may prove helpful in avoiding toxicity in healthy tissues adjacent to tumors, thereby offering a reasonable level of safety. Our findings might support the potential for clinical application of this siRNA delivery system to treat aggressive relapsed gastric cancer.

Previous studies have reported several Smo antagonists to block Hh signaling for cancer treatment, such as cyclopamine,[49] GDC-0449,[50] IPI-926,[51] and Smo siRNA.[52] Although this is a reasonable approach, it is limited because tumors with acquired mutations in Smo or downstream components will likely fail to respond to Smo antagonists.[53] Moreover, another report has demonstrated that polyethyleneimine-spherical nucleic acid nanoparticles loaded with Gli1 siRNA reduce the growth of stem-like neurospheres and sensitize glioblastoma to temozolomide chemotherapy in vitro.[54] A similar study has shown that the Gli1 inhibitor GANT61 potently inhibits the proliferation of a CD34+ subpopulation of acute myeloid leukemia cells and enhances sensitivity to cytarabine.[55] These findings also indicate that the inhibition of transcriptional activity of Gli1 in CSCs may be a potential strategy for cancer therapy. Consistent with those studies, our findings demonstrate the potential antitumor bioactivity of the targeting Gli1 siRNA nanoparticles by selectively targeting CD44 and blocking Gli1-mediated Hh signaling.

There are several limitations to our study. First, we chose only one in vitro and in vivo gastric CSC model. To more accurately verify the current findings, additional cell lines and tumor models should be selected to examine the effect of the targeting Gli1 siRNA nanoparticles delivery system on a wider range of applications. Second, CSCs play a crucial role in the recurrence and metastasis of cancer. In this study, the in vivo experiments were examined only in the recurrence model of gastric CSCs; hence, further pharmacodynamic evaluation is required for the cancer metastatic model arising from gastric CSCs. Third, in terms of the molecular mechanism, we only investigated the protein levels of Gli1 following treatment with various formulations in Western blot analysis. In future, it would be useful to perform mechanistic studies to further investigate Hh signaling components (Shh, Ptch, Smo), cancer stemness genes (Oct4, Sox2, Snail) and downstream target genes (cyclin D1, c-Myc and Bcl-2) using more techniques.

Conclusions

In summary, targeting Gli1 siRNA nanoparticles were designed and developed to selectively eliminate gastric CSCs for dual-targeting CD44 and Gli1. DSPE-HA single-point conjugates were prepared and subsequently coupled on the surface of the Gli1 siRNA nanoparticles to generate our targeted delivery system for therapeutic siRNAs that were specifically guided to CD44+ CSCs. In vitro and in vivo studies revealed that the targeting Gli1 siRNA nanoparticles were specifically and stably enriched in the tumor mass, selectively eliminated gastric CSCs, and consequently exhibited superior therapeutic efficacy. This novel targeted agent may serve as a promising drug for preventing recurrence and metastasis of gastric cancer in future. The approach of nanoparticle delivery system via DSPE-HA single-point conjugates provides insights into potential technique platforms to facilitate the delivery of therapeutic siRNAs to gastric CSCs.

Funding

This work was supported by the National Natural Science Foundation of China [NSFC 81302728, 81472787, 81773671, and 81828010]; CAMS Innovation Fund for Medical Sciences [CIFMS 2016-I2M-3-013]; The Drug Innovation Major Project of China [2018ZX09711001-007-002].

Disclosure

Liang Li reports a patent pending: A targeted nucleic acid drug and a preparation method and use thereof. Patent Application No.: 2019111166183 Chinese Patent, 2019/11/15. The authors declare no other potential conflicts of interest in this work.

References

1. Bray F, Ferlay J, Soerjomataram I, et al. Global cancer statistics 2018: GLOBOCAN estimates of incidence and mortality worldwide for 36 cancers in 185 countries. *CA Cancer J Clin*. 2018;68:394–424. doi:10.3322/caac.21492
2. Rocco A, Compare D, Nardone G. Cancer stem cell hypothesis and gastric carcinogenesis: experimental evidence and unsolved questions. *World J Gastrointest Oncol*. 2012;4:54–59. doi:10.4251/wjgo.v4.i3.54
3. Nakamura K, Iinuma H, Aoyagi Y, et al. Predictive value of cancer stem-like cells and cancer-associated genetic markers for peritoneal recurrence of colorectal cancer in patients after curative surgery. *Oncology*. 2010;78(5–6):309–315. doi:10.1159/000318862
4. Dean M, Fojo T, Bates S. Tumour stem cells and drug resistance. *Nat Rev Cancer*. 2005;5:275–284. doi:10.1038/nrc1590
5. Sun M, Zhou W, Zhang YY, et al. CD44+ gastric cancer cells with stemness properties are chemoradioresistant and highly invasive. *Oncol Lett*. 2013;5:1793–1798. doi:10.3892/ol.2013.1272
6. Takaishi S, Okumura T, Tu S, et al. Identification of gastric cancer stem cells using the cell surface marker CD44. *Stem Cells*. 2009;27:1006–1020. doi:10.1002/stem.30
7. Zhang C, Li C, He F, et al. Identification of CD44+ CD24+ gastric cancer stem cells. *J Cancer Res Clin Oncol*. 2011;137:1679–1686. doi:10.1007/s00432-011-1038-5
8. Chen T, Yang K, Yu J, et al. Identification and expansion of cancer stem cells in tumor tissues and peripheral blood derived from gastric adenocarcinoma patients. *Cell Res*. 2012;22:248–258. doi:10.1038/cr.2011.109
9. Senel F, Kökenek Unal TD, Karaman H, et al. Prognostic value of cancer stem cell markers CD44 and ALDH1/2 in gastric cancer cases. *Asian Pac J Cancer Prev*. 2017;18:2527–2531. doi:10.22034/APJCP.2017.18.9.2527
10. Ibrahim HM, AbdElbary AM, Mohamed SY, et al. Prognostic value of cyclin D1 and CD44 expression in gastric adenocarcinoma. *J Gastrointest Cancer*. 2019;50(3):370–379. doi:10.1007/s12029-018-0079-2
11. Chen Y, Fu Z, Xu S, et al. The prognostic value of CD44 expression in gastric cancer: a meta-analysis. *Biomed Pharmacother*. 2014;68:693–697. doi:10.1016/j.biopha.2014.08.001
12. Gupta B, Poudel BK, Ruttala HB, et al. Hyaluronic acid-capped compact silica-supported mesoporous titania nanoparticles for ligand-directed delivery of doxorubicin. *Acta Biomater*. 2018;80:364–377. doi:10.1016/j.actbio.2018.09.006
13. Peer D, Margalit R. Loading mitomycin C inside long circulation hyaluronan targeting nano-liposomes increases its antitumor activity in three mice tumor models. *Int J Cancer*. 2004;108:780–789. doi:10.1002/ijc.11615
14. Mizrahy S, Raz SR, Hasgaard M, et al. Hyaluronan-coated nanoparticles: the influence of the molecular weight on CD44-hyaluronan interactions and on the immune response. *J Control Release*. 2011;156(2):231–238. doi:10.1016/j.jconrel.2011.06.031
15. Bhuria V, Xing J, Scholta T, et al. Hypoxia induced Sonic Hedgehog signaling regulates cancer stemness, epithelial-to-mesenchymal transition and invasion in cholangiocarcinoma. *Exp Cell Res*. 2019;385(2):111671. doi:10.1016/j.yexcr.2019.111671
16. Yoon C, Park DJ, Schmidt B, et al. CD44 expression denotes a subpopulation of gastric cancer cells in which Hedgehog signaling promotes chemotherapy resistance. *Clin Cancer Res*. 2014;20(15):3974–3988. doi:10.1158/1078-0432.CCR-14-0011
17. Zhao C, Chen A, Jamieson CH, et al. Hedgehog signaling is essential for maintenance of cancer stem cells in myeloid leukaemia. *Nature*. 2009;458(7239):776–779. doi:10.1038/nature07737
18. Chang WH, Lai AG. Aberrations in Notch-Hedgehog signalling reveal cancer stem cells harbouring conserved oncogenic properties associated with hypoxia and immunoevasion. *Br J Cancer*. 2019;121:666–678. doi:10.1038/s41416-019-0572-9
19. Cochrane CR, Szczepny A, Watkins DN, et al. Hedgehog signaling in the maintenance of cancer stem cells. *Cancers (Basel)*. 2015;7:1554–1585. doi:10.3390/cancers7030851
20. Justilien V, Fields AP. Molecular pathways: novel approaches for improved therapeutic targeting of Hedgehog signaling in cancer stem cells. *Clin Cancer Res*. 2015;21:505–513. doi:10.1158/1078-0432.CCR-14-0507
21. Takebe N, Harris PJ, Warren RQ, et al. Targeting cancer stem cells by inhibiting Wnt, Notch, and Hedgehog pathways. *Nat Rev Clin Oncol*. 2011;8:97–106. doi:10.1038/nrclinonc.2010.196
22. Faião-Flores F, Alves-Fernandes DK, Pennacchi PC, et al. Targeting the hedgehog transcription factors GLI1 and GLI2 restores sensitivity to vemurafenib-resistant human melanoma cells. *Oncogene*. 2017;36(13):1849–1861. doi:10.1038/onc.2016.348
23. Xu M, Gong A, Yang H, et al. Sonic hedgehog-glioma associated oncogene homolog 1 signaling enhances drug resistance in CD44(+)/Musashi-1(+) gastric cancer stem cells. *Cancer Lett*. 2015;369:124–133. doi:10.1016/j.canlet.2015.08.005
24. Amable L, Fason J, Gavin E, et al. Gli1 contributes to cellular resistance to cisplatin through altered cellular accumulation of the drug. *Oncol Rep*. 2014;32(2):469–474. doi:10.3892/or.2014.3257
25. Zahreddine HA, Culjkovic-Kraljacic B, Assouline S, et al. The sonic Hedgehog factor GLI1 imparts drug resistance through inducible glucuronidation. *Nature*. 2014;511(7507):90–96. doi:10.1038/nature13283
26. Liao ZQ, Ye M, Yu PG, et al. Glioma-Associated Oncogene Homolog1 (Gli1)-Aquaporin1 pathway promotes glioma cell metastasis. *BMB Rep*. 2016;49:394–399. doi:10.5483/BMBRep.2016.49.7.011
27. Santini R, Vinci MC, Pandolfi S, et al. Hedgehog-GLI signaling drives self-renewal and tumorigenicity of human melanoma-initiating cells. *Stem Cells*. 2012;30:1808–1818. doi:10.1002/stem.1160
28. Papadopoulos V, Tsapakidis K, Riobo Del Galdo NA, et al. The prognostic significance of the Hedgehog signaling pathway in colorectal cancer. *Clin Colorectal Cancer*. 2016;15:116–127. doi:10.1016/j.clcc.2016.02.010
29. Xu Y, Song S, Wang Z, et al. The role of hedgehog signaling in gastric cancer: molecular mechanisms, clinical potential, and perspective. *Cell Commun Signal*. 2019;17:157. doi:10.1186/s12964-019-0479-3
30. Khalil IA, Yamada Y, Harashima H. Optimization of siRNA delivery to target sites: issues and future directions. *Expert Opin Drug Deliv*. 2018;15:1053–1065. doi:10.1080/17425247.2018.1520836
31. Kim B, Park JH, Sailor MJ. Rekindling RNAi therapy: materials design requirements for in vivo siRNA delivery. *Adv Mater*. 2019;31:e1903637. doi:10.1002/adma.201903637
32. Lee J, Cho YJ, Lee JW, et al. KSP siRNA/paclitaxel-loaded PEGylated cationic liposomes for overcoming resistance to KSP inhibitors: synergistic antitumor effects in drug-resistant ovarian cancer. *J Control Release*. 2020;321:184–197. doi:10.1016/j.jconrel.2020.02.013
33. Ruhela D, Kivimäe S, Szoka FC. Chemoenzymatic synthesis of oligohyaluronan- lipid conjugates. *Bioconjug Chem*. 2014;25:718–723. doi:10.1021/bc4005975

34. Saadat E, Amini M, Khoshayand MR, et al. Synthesis and optimization of a novel polymeric micelle based on hyaluronic acid and phospholipids for delivery of paclitaxel, in vitro and in-vivo evaluation. *Int J Pharm*. 2014;475:163–173. doi:10.1016/j.ijpharm.2014.08.030
35. Ruhela D, Riviere K, Szoka FCJ. Efficient synthesis of an aldehyde functionalized hyaluronic acid and its application in the preparation of hyaluronan-lipid conjugates. *Bioconjug Chem*. 2006;17:1360–1363. doi:10.1021/bc0600721
36. Saadat E, Amini M, Dinarvand R, et al. Polymeric micelles based on hyaluronic acid and phospholipids: design, characterization, and cytotoxicity. *J Appl Polym Sci*. 2014;131:40944. doi:10.1002/app.40944
37. Liu D, Lian Y, Fang Q, et al. Hyaluronic-acid-modified lipid-polymer hybrid nanoparticles as an efficient ocular delivery platform for moxifloxacin hydrochloride. *Int J Biol Macromol*. 2018;116:1026–1036. doi:10.1016/j.ijbiomac.2018.05.113
38. Stewart JC. Colorimetric determination of phospholipids with ammonium ferrothiocyanate. *Anal Biochem*. 1980;104:10–14. doi:10.1016/0003-2697(80)90269-9
39. Barat S, Chen X, Cuong BK, et al. Gamma-Secretase Inhibitor IX (GSI) impairs concomitant activation of notch and wnt-Beta-Catenin pathways in CD44+ gastric cancer stem cells. *Stem Cells Transl Med*. 2017;6:819–829. doi:10.1002/sctm.16-0335
40. Zhu P, Fan Z. Cancer stem cells and tumorigenesis. *Biophys Rep*. 2018;4:178–188. doi:10.1007/s41048-018-0062-2
41. Takebe N, Miele L, Harris PJ, et al. Targeting Notch, Hedgehog, and Wnt pathways in cancer stem cells: clinical update. *Nat Rev Clin Oncol*. 2015;12:445–464. doi:10.1038/nrclinonc.2015.61
42. Ingham PW, Nakano Y, Seger C. Mechanisms and functions of Hedgehog signaling across the metazoan. *Nat Rev Genet*. 2011;12:393–406. doi:10.1038/nrg2984
43. Sari IN, Phi LTH, Jun N, et al. Hedgehog signaling in cancer: a prospective therapeutic target for eradicating cancer stem cells. *Cells*. 2018;7:E208. doi:10.3390/cells7110208
44. Yao HJ, Zhang YG, Sun L, et al. The effect of hyaluronic acid functionalized carbon nanotubes loaded with salinomycin on gastric cancer stem cells. *Biomaterials*. 2014;35:9208–9223. doi:10.1016/j.biomaterials.2014.07.033
45. Banerji S, Wright AJ, Noble M, et al. Structures of the CD44-hyaluronan complex provide insight into a fundamental carbohydrate-protein interaction. *Nat Struct Mol Biol*. 2007;14:234–239. doi:10.1038/nsmb1201
46. Nelson CE, Kintzing JR, Hanna A, et al. Balancing cationic and hydrophobic content of PEGylated siRNA polyplexes enhances endosome escape, stability, blood circulation time, and bioactivity in vivo. *ACS Nano*. 2013;7:8870–8880. doi:10.1021/nn403325f
47. Ahmad A, Khan JM, Haque S. Strategies in the design of endosomolytic agents for facilitating endosomal escape in nanoparticles. *Biochimie*. 2019;160:61–75. doi:10.1016/j.biochi.2019.02.012
48. Björnmalm M, Thurecht KJ, Michael M, et al. Bridging bio-nano science and cancer nanomedicine. *ACS Nano*. 2017;11:9594–9613. doi:10.1021/acsnano.7b04855
49. Gutzmer R, Solomon JA. Hedgehog pathway inhibition for the treatment of basal cell carcinoma. *Target Oncol*. 2019;14:253–267. doi:10.1007/s11523-019-00648-2
50. LoRusso PM, Rudin CM, Reddy JC, et al. Phase I trial of Hedgehog pathway inhibitor vismodegib (GDC-0449) in patients with refractory, locally advanced or metastatic solid tumors. *Clin Cancer Res*. 2011;17:2502–2511. doi:10.1158/1078-0432.CCR-10-2745
51. Olive KP, Jacobetz MA, Davidson CJ, et al. Inhibition of Hedgehog signaling enhances delivery of chemotherapy in a mouse model of pancreatic cancer. *Science*. 2009;324:1457–1461. doi:10.1126/science.1171362
52. Yang B, Sun HY, Chen WH, et al. Lentivirus-mediated SMO RNA interference inhibits SMO expression and cell proliferation, and affects the cell cycle in LNCaP and PC3 cancer cell lines. *Asian J Androl*. 2010;12:196–202. doi:10.1038/aja.2009.79
53. Das S, Samant RS, Shevde LA, et al. Nonclassical activation of Hedgehog signaling enhances multidrug resistance and makes cancer cells refractory to smoothened-targeting Hedgehog inhibition. *J Biol Chem*. 2013;288:11824–11833. doi:10.1074/jbc.M112.432302
54. Melamed JR, Ioele SA, Hannum AJ, et al. Polyethylenimine-Spherical nucleic acid nanoparticles against Gli1 reduce the chemoresistance and stemness of glioblastoma cells. *Mol Pharm*. 2018;15:5135–5145. doi:10.1021/acs.molpharmaceut.8b00707
55. Long B, Wang LX, Zheng FM, et al. Targeting GLI1 suppresses cell growth and enhances chemosensitivity in CD34+ enriched acute myeloid leukemia progenitor cells. *Cell Physiol Biochem*. 2016;38:1230–1288. doi:10.1159/000443075